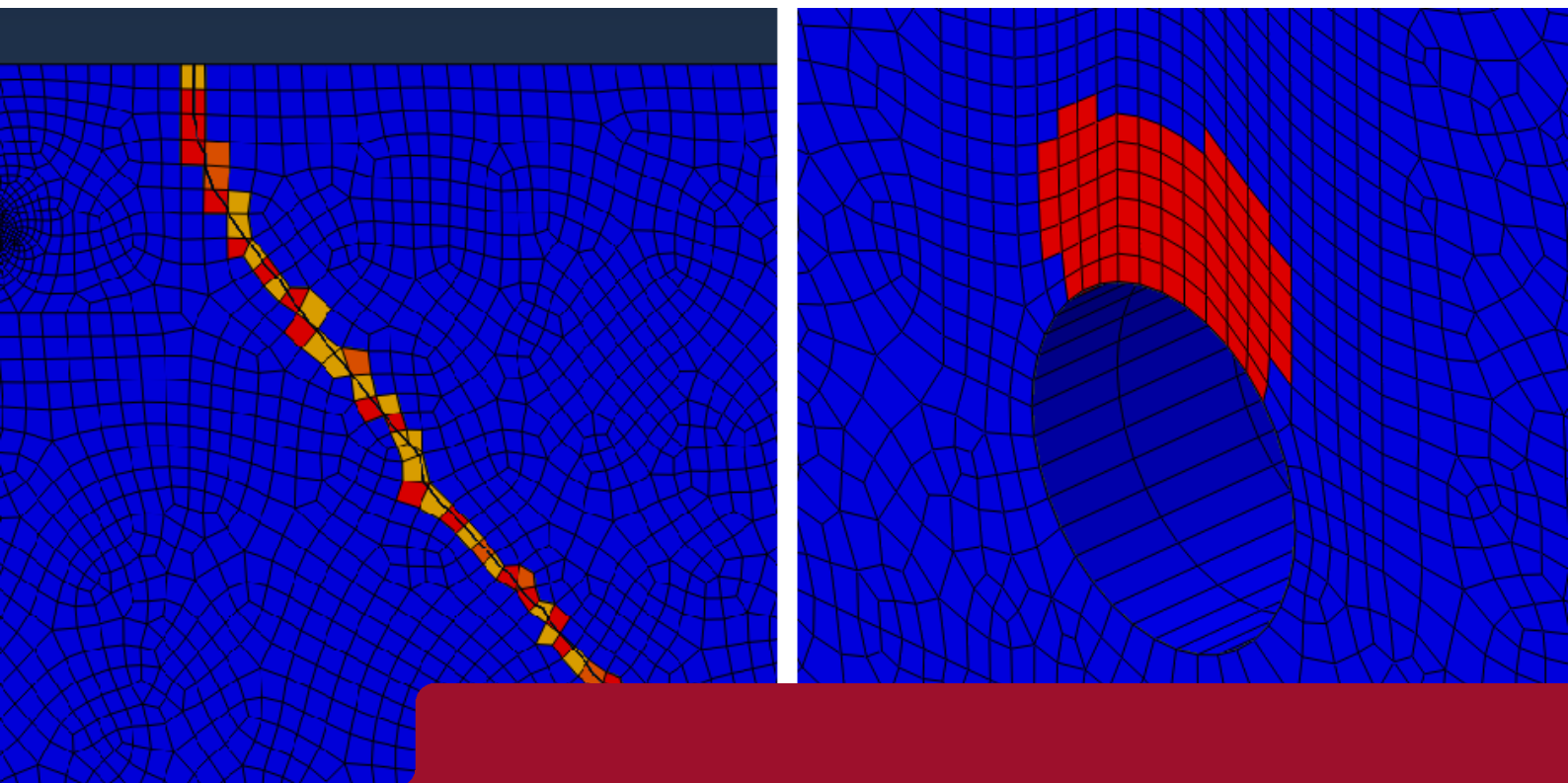




DEGREE PROJECT IN VEHICLE ENGINEERING,
SECOND CYCLE, 30 CREDITS
STOCKHOLM, SWEDEN 2018

An Attempt Towards FE-Modelling of Fracture Propagation in Railway Wheels

FRED ÖHNANDER



KTH ROYAL INSTITUTE OF TECHNOLOGY
SCHOOL OF ENGINEERING SCIENCES

Preface

This thesis is part of my Degree of Master of Science in Engineering in the field Vehicle Engineering and is performed at the Division of Railway Technology, Department of Aeronautical and Vehicle Engineering at the Royal Institute of Technology (KTH) in Stockholm. The thesis is part of the FR8RAIL project arranged by the European rail initiative Shift2Rail. The thesis has been carried out in cooperation with CAF MiiRA which is dedicated to the design and manufacture of rail vehicle components.

Firstly, I would like to thank my supervisors Carlos Casanueva and Saeed Hossein-Nia for their guidance in the work. Especially I would like to thank Saeed for your enthusiasm for the project and for pushing me forward in the right direction. I also appreciate the literature suggestions given by both Carlos and Saeed.

As a novice in Abaqus I have needed substantial help from people with experience with it. Here, I would like to thank Farshad Shafieian, CAE Engineer at Scania Group, Anton Shipsha, PhD student at KTH, and Per-Anders Jönsson, CEO for Tikab Strukturmekanik AB, for all their help with answering my questions regarding Abaqus. I would also like to thank Anton for your help in both explaining, as well as finding valuable information, about the fundamentals of fracture mechanics.

I would also like to thank my master thesis colleagues for their feedback from the master thesis presentations as well as the rest of the people in the department for their company and discussions of both engineering subjects as well as various other discussions.

Finally, I would like to thank the love of my life, Sara, for all the encouragement and positivity you bring when I am down. You are my best friend and you make me smile and laugh almost every single day.

Fred Öhnander
ohnander@kth.se

Stockholm, June 2018

Abstract

The demand for higher velocities and heavier axle loads for freight trains leads to higher forces on the railway wheels which in turn lead to an increase in stresses on and below the surface of the wheel-rail contact. By time, this induces wear on the wheels which consequently lead to higher maintenance costs and in some cases accidents. The ability to predict the evolution of wheel profiles due to uniform wear has been demonstrated with a rather accurate precision in most operational conditions. These wear models are based on wear coefficients and since they are not usually valid for real operational conditions, the models are generally calibrated against real-life scenarios in order to adjust the coefficients from test conditions to real-life lubrication conditions. This engineering approach can be useful in prediction of wear in systems where the materials and contact conditions do not vary. However, when addressing material development focused on reducing specific damage modes, the approach is of limited use because the obtained wear coefficients are not directly related to material properties. Therefore, attempts towards developing physical fracture propagation models that relates to the contact conditions and material properties have been made. The purpose has been to retrieve vital information about where a fracture initiates and how it propagates. In the long run, it is of great interest to be able to attain information about how a material particle is removed from the contact surface. Studies for this type of model was done in the 70's and 80's mainly with pin-disk experiments but has not been utilized in the specific field of wheel-rail contact. The thesis is part of the FR8RAIL project arranged by the European rail initiative Shift2Rail. Literature studies have been the basis for the thesis in order to gain vital insights into fracture mechanics and other related fields. The physical fracture propagation models have been constructed in the FE software Abaqus with the implementation of the XFEM. For the 2D model, the fracture initiates at the top of the implanted inclusion when the friction coefficient is $\mu \leq 0.2$ and propagates upwards a few elements. For $\mu > 0.2$, the fracture initiates at the right surface boundary where the pressure distribution and traction is applied. The fracture propagation angle increases relative to the surface as the friction coefficient value is increased. The fracture for the 3D model extends broader compared to the 2D model at the top of the inclusion in the case of $\mu \leq 0.2$. The fracture initiates at the same surface location as for the 2D model for $\mu > 0.2$. The fracture propagation is however non-existent due to convergence problems. The FE-models constructed are initial steps towards analysing the fracture propagation and closely related phenomena for a railway freight wheel in detail. At the end of the thesis, the simplified models give mainly information about the fracture initiation, propagation and its patterns. From this first phase, further adjustments and improvements can take place in order to eliminate the margins of error. In the long run, fully integrated models with further implementations such as detailed microstructure for the contact conditions, plastic behaviour for the material, and complete three-dimensional models can finally be employed.

Keywords: railway wheel, wheel-rail contact, wear, fracture initiation, physical fracture propagation model, FE-model, fracture mechanics, XFEM, inclusion.

Sammanfattning

Efterfrågan på högre hastigheter och tyngre axelbelastningar för godståg leder till högre krafter på järnvägshjulen som i sin tur leder till ökade spänningar på och under ytan vid hjul-räl-kontakten. Med tiden induceras slitage på hjulen som följdaktligen leder till höga underhållskostnader och i vissa fall olyckor. Förmågan att förutse utvecklingen av hjulprofiler på grund av enhetligt slitage har visats kunna ske med en noggrann precision under de flesta driftsförhållanden. Dessa slitagemodeller bygger på slitagekoefficienter, och eftersom de vanligtvis inte är giltiga under realistiska driftsförhållanden är modellerna i allmänhet kalibrerade mot verkliga händelseförlopp för att justera koefficienterna från testförhållandena till realistiska smörjförhållanden. Detta tekniska tillvägagångssätt kan vara användbart vid prognos av slitage i system där material och kontaktförhållanden inte varierar. När man addresserar materialutveckling inriktad på att reducera specifika skadelägen är emellertid tillvägagångssättet av begränsad användning eftersom de erhållna slitagekoefficienterna inte är direkt relaterade till materialegenskaper. Därför har försök gjorts till att utveckla fysikaliska sprickbildningsmodeller som relateras till kontaktförhållanden och materialegenskaper. Syftet har varit att erhålla viktig information om var en spricka initieras och hur den fortskrider. I det långa loppet är det även av stor vikt att kunna erhålla information om hur en materialpartikel avlägsnas från kontaktytan. Studier för denna typ av modeller har gjorts på 70- och 80-talet i huvudsak med stift- och skivexperiment men har inte använts inom det specifika området för hjul-räl-kontakt. Avhandlingen ingår i FR8RAIL-projektet som arrangeras av det europeiska järnvägsinitiativet Shift2Rail. Literaturstudier har varit grunden för avhandlingen för att få väsentlig insikt i frakturmekanik och andra relaterade områden. De fysiska sprickbildningsmodellerna har konstrueras i FE-mjukvaran Abaqus med XFEM som implementering. För 2D-modellen initieras sprickan överst vid den implanterade imperfektionen när friktionskoefficienten är $\mu \leq 0.2$ och propagerar uppåt några få element. För $\mu > 0.2$ initieras sprickan på högra ytgränsen där tryckfördelning och friktionskraft appliceras. Utbredningsvinkeln för sprickan ökar relativt till ytan då friktionskoefficienten ökar. Sprickan för 3D-modellen breder ut sig mer jämfört med 2D-modellen överst vid imperfektionen då $\mu \leq 0.2$. Sprickan initieras på samma ytplats som för 2D-modellen vid $\mu > 0.2$. Sprickbildningen är dock obefintlig på grund av konvergensproblem. De konstruerade FE-modellerna är initiala steg mot att analysera sprickutbredningen och närbesläktade fenomen för ett godstågs järnvägshjul i detalj. I slutet av avhandlingen ger de förenklade modellerna huvudsakligen information om sprickinitiering, utbredning och dess mönster. Ytterligare justeringar och förbättringar kan ske efter denna första fas i syfte att eliminera felmarginerna. På lång sikt kan slutligen helt integrerande modeller med ytterligare implementeringar såsom detaljerad mikrostruktur för kontaktförhållandena, oelastiskt materialbeteende och kompletta tredimensionella modeller användas.

Nyckelord: järnvägshjul, hjul-räl-kontakt, slitage, sprickinitiering, fysisk sprickbildningsmodell, FE-modell, frakturmekanik, XFEM, imperfektion.

Table of Contents

PREFACE	I
ABSTRACT	II
SAMMANFATTNING	III
1 INTRODUCTION.....	1
2 WEAR	3
2.1 Introduction	3
2.2 Adhesive Wear Mechanisms	4
2.3 Wear-Regime Map for Metals.....	5
2.4 Delamination Wear	7
3 CONTACT MECHANICS.....	9
3.1 Hertzian Line Contact in Full-Slip	9
4 FRACTURE MECHANICS	13
4.1 Crack Initiation.....	13
4.2 The Stress Intensity Approach	14
4.3 Effect of Specimen Geometry	17
4.4 Linear Elastic Fracture Mechanics (LEFM).....	20
4.5 Elasto-Plastic Fracture Mechanics (EPFM)	20
4.6 Extended Finite Element Method (XFEM)	21
5 FE-MODELLING	24
5.1 2D Model.....	25
5.2 3D Model.....	27
6 RESULTS AND DISCUSSIONS	29

6.1	2D Model.....	29
6.2	3D Model.....	34
6.3	General	35
7	CONCLUSIONS	37
8	FUTURE WORK AND RESEARCH	38
	REFERENCES	40

1 Introduction

The demand for higher velocities and heavier axle loads for freight trains leads to higher forces on the railway wheels. The increase of forces leads in turn to an increase in stresses on the surface and below the surface of the wheel-rail contact. By time, this induces wear on the wheels which consequently lead to higher maintenance costs and in some cases accidents. Thus, for the safety aspect as well as for the future prospect of freight trains and its competitiveness, there is a desire to reduce the maintenance required.

Nowadays, models that predict the wheel profile evolution have been demonstrated the ability to predict with a rather accurate precision the evolution of wheel and rail profiles due to uniform wear in most operational conditions. These wear models are based on wear coefficients, where removal of material in the wheel-rail contact is related to a coefficient which depends on a set of contact conditions. In order to obtain the wear coefficients experimentally, various laboratory tests have been carried out. Yet, analyses of these coefficients demonstrate their invalidity for real operational conditions. Thus, the models are generally calibrated against real-life scenarios in order to adjust the coefficients from test conditions to real-life lubrication conditions. This engineering approach can be useful in prediction of wear in systems where the materials and contact conditions do not vary. However, when addressing material development in the focus on reducing specific damage modes, the approach is of limited use. This is because the obtained wear coefficients are not directly related to material properties.

In the pursuance of solving this kind of problem, it is of great necessity to develop physical fracture propagation models that relates to the contact conditions and material properties. The aim is to utilize the models for the sake of retrieving vital information about where a fracture initiates and how it propagates. Specifically, different propagation patterns alongside with typical positions on the railway wheel where cracks usually initiate is of great importance. In the long run, it is of great interest to be able to attain information about how a material particle is removed from the contact surface. Additionally, valuable results such as wear in form of loss of material volume or dissipation of energy per distance travelled are of great significance alongside with knowledge about how the pressure distribution and friction force in the contact surface relates to certain phenomena. Studies for this type of model was done in the 70's and 80's mainly with pin-disk experiments but has not been utilized in the specific field of wheel-rail contact.

The thesis is part of the FR8RAIL project arranged by the European rail initiative Shift2Rail. Shift2Rail aims at accelerating the integration of new and advanced technologies into innovative rail product solutions. The initiatives' ambitions in the long run is to double the capacity of the European rail system, increase its reliability and service quality by 50% while at the same time reducing the life-cycle costs by also 50% [1]. The FR8RAIL project is about the development of functional requirements for sustainable and attractive European rail freight. The project aims at developing track friendly and low maintenance freight wagons. The development of new types of running gear concepts that will reduce wheel-rail contact

forces is one strategy to achieve this. The specific goals of the FR8RAIL project are to reduce the cost of freight transport measured by tonnes per km by 10%, reduce the time variations during dwelling by 20%, and increase attractiveness of logistic chains by making available 100% of the rail freight transport information to logistic chain information systems [2].

It is of great necessity and importance to streamline the fracture propagation model in order for it to work properly and for it to be flexible to different input data. There is also of great significance to make simplifications in order to be able to achieve the desired result in the given time frame. A relatively large block which encompasses the contact patch will be used in order to reduce the influence of reaction forces from the boundaries. The rails will be seen as being idealized with smooth surface roughness which will imply that no asperities are related to the material surface of the rails. This simplification makes the application process of the pressure distribution and friction force to the wheel contact surface under study much more straightforward. The distribution and traction are based on Hertzian theory where only full-slip condition for the sliding is assumed. Only the tread of the wheel will be taking into account, disregarding flange contact. The location of the wheel-rail contact stresses is the same for every load cycle. The plastic behaviour of the material is neglected and therefore the behaviour of the material is only elastic.

Literature studies will start off the project in order to gain vital insights of for instance the fundamentals of wear, fracture mechanics and software techniques and strategies. The physical fracture propagation models will be constructed in the finite element and computer-aided engineering software called Abaqus. For the fracture analyses, the extended finite element method (XFEM) which is implemented into Abaqus, is utilized.

The project can be divided into two larger sections; theory and simulation. The theory will start off with a chapter of *wear* which will include adhesive wear mechanisms, wear-regime map for metals and delamination wear. This is followed up with a chapter about *contact mechanics* which go into detail about the Hertzian line contact in full-slip. Thereafter, an extensive chapter about the fundamentals of *fracture mechanics* will be presented. In this chapter, the reason for cracks to initiate will be discussed alongside with the energy-balance approach, the stress intensity approach, the effect of specimen geometry as well as methods to analyse fracture growth together with the XFEM. The pre-processing of the simulations will then be described in the chapter *FE-modelling*. Here, the processes of constructing the physical fracture propagation models of a simplified railway wheel in ABAQUS will be explained. The results of the simulations are presented and interpreted in the upcoming *results and discussions* chapter. From the discussions, some conclusions have been made and are explained in the chapter *conclusions*. Finally, what should be done in order to further improve the fracture propagation models created is discussed in the *future work and research* chapter.

2 Wear

The goal of this thesis is to create fracture propagation models that can relate to contact conditions and material properties. In the future however, in order to gain vital insights about the removal of the material, the models need to account for wear related phenomena. Furthermore, adhesive wear is of great importance when considering the detailed microstructure of the wheel surface. The wear-regime map is useful for depicting the various regimes in which different modes of wear dominate. Therefore, the fundamentals of wear are presented in this chapter followed by adhesive wear mechanisms and wear-regime map for metals. Finally, due to its relation to adhesive wear and its great influence on wheel and rail wear, delamination wear will conclude this chapter.

2.1 Introduction

Railway vehicles use friction to transfer forces in the wheel-rail contact surface. Pressure and friction forces are making it possible for the wheel-sets to follow a certain track and be able to accelerate and brake. There is however creep forces that are arising from sliding motions between the wheel and the rail as the wheels are running along the track. The main two phenomena that causes changes in the geometrical shape of the wheel is material removal and material subjected to plastic deformation. Flange wear is caused mainly by curve negotiation alongside with stiff wheel-sets that contribute to higher yaw angles relative to the track. The tread wear however is caused by the normal forces from the wheel-rail contact combined with creepages and creep forces but also traction and braking forces [3].

Wear can from a tribology point of view be defined as the damage to a solid surface involving continuous loss of material and repositioning of material in the case of two surfaces interacting through a relative motion. There are many different influences to material wear and it lies not only in the sole properties of the material but also in the geometry of the bodies in contact, surface roughness, loading, lubrication and environment. There are usually complicated mechanisms that causes these wear damages and many times they are indistinguishable from one another. However, the main mechanisms that are wheel-rail related are [4]:

There are mainly four different mechanical wear types:

- *Abrasive wear* – Is the cutting on the surface by hard particles or hard asperities against each other.
- *Adhesive wear* – Is the removal of material due to adhesion between the wheel and rail surfaces.
- *Corrosive wear* – Corrosive wear occurs when there is abrasive and adhesive wear in a corrosive environment.
- *Rolling contact fatigue (RCF)* – Occurs when continuous and repeated application of a load (cyclic loading) on a material eventually degrades it and finally leads to fatigue. To be more specific, the cyclic loading can induce surface or subsurface cracks [3] [4].

The rolling contact fatigue of the wheels is often categorized based on the distance of where the cracks are initiated compared to the surface of the wheel. These are:

- *Surface initiated fatigue*
- *Sub-surface initiated fatigue* (3-10 mm from the surface)
- *Deep-surface initiated fatigue* (10-25 mm from the surface)

The sub-surface and deep-surface cracks are quite rare, yet these two are the most dangerous ones when compared to the surface cracks and might cause derailments. Where there exist a low fatigue resistance of the material such as microscopic manganese sulphide inclusions (sub-surface) and voids (deep-surface), there are great risks for both of the phenomena to occur. Surface initiated cracks are conversely often harmless and easy to cope with and oftentimes dealt with through reprofiling of the wheel profiles or even by regular natural wear. However, reprofiling is costly, especially when it interrupts the operation of the trains. It may also escalate the track degradation that is caused by high impact forces [4].

2.2 Adhesive Wear Mechanisms

This section is mainly based on *Wear Analysis for Engineers* by Raymond G. Bayer [5].

The rudimentary concept for adhesive mechanisms is that the contact between the surfaces occurs at discrete points within the apparent area of contact. These points, that are called junctions, are bonding between the surface asperities. If the two surfaces move in relation to each other, the junctions get broken and new ones are formed. Where the bond is strong enough the fracture will occur within the weaker asperity. Otherwise the separation will take place at the interface between the asperities. The transferred material may as a result of stored elastic energy detach itself once the separation has occurred. Or it might even become detached as a result of subsequent contact which forms loose particle-like wear debris. Usually, large quantities of plastic deformation are associated with these mechanisms.

Regarding these types of mechanisms, the primary wear scar feature that is indicative is the presence of transferred material. This transferred material is usually in the form of attached and highly deformed chunks. The wear debris is the secondary feature form. It should be highly deformed and particle-like, rather than platelets or flakes, for adhesive mechanisms. However, in all cases of adhesive wear, these features may not be observed since the material that is transferred can be detached from surfaces and the shape of wear debris can be altered after it is formed. The specific form of Archard's wear equation that is commonly used for adhesive wear is the following:

$$V = \frac{K}{3} \frac{PS}{p} \quad (2.1)$$

Where V is the volume of wear, P is the load, S is the distance of sliding, and p is the penetration hardness of the softer material. The probability of transfer at junction is defined as K .

The tendency for which adhesive wear to occur can be associated with the properties of the two materials in contact and the state of their surfaces. Generally, it can be noted that properties or conditions that ensure that the formation of strong bonds are enhanced between the two surfaces will increase the probability of adhesive wear. Correspondingly, certain conditions that tend to inhibit the bonding between surfaces decrease the probability of adhesive wear. Factors that tend to increase the probability of adhesive wear are high surface energy, similar crystal structure, chemical affinity and mutual solubility. Surface contamination, oxides and lubricants often tend to reduce the probability of adhesive wear.

The contact pressure has also an impact on the tendency for adhesive wear and the value of K apart from the material factors mentioned earlier. A reduced contact pressure has a tendency to also reduce K . For transfer to occur a minimum contact pressure is needed. Adhesive mechanisms may or may not be significant in different tribosystems, it all depends on the influence of different factors such as material properties, surface conditions and contact stress.

Bonding is the distinguishing feature of adhesive wear mechanisms. It is however not the necessarily the only phenomenon that can be involved. For adhesive wear the probability of transfer is mainly affected by the relative strength of the bond to the strength of the asperity or surface. The transfer does not occur if the bond is weaker. Therefore, possible factors in adhesive wear behaviour are processes that affect the strength of either the bond or the asperity. In different tribosystems, some different examples of phenomena that may affect the significance of adhesive wear are oxide formation, work hardening, crack formation and thermal softening. The stronger the bond is, the more force it takes to separate the junction.

Severe adhesive wear is possible for conditions like unlubricated sliding between self-mated metals and unlubricated sliding between different metals. Generally the tendency for adhesive wear is considered to be the highest among these conditions. For metal-non-metal pairs, non-metal pairs and lubricated pairs the tendency is substantially reduced. Any adhesive wear mechanism is likely to fall under the *mild* category for these combinations. The common engineering tool for reducing adhesive wear between materials is lubrication.

2.3 Wear-Regime Map for Metals

The foundation of this subchapter has been retrieved from *Tribology – Friction and Wear of Engineering Materials* by I. M. Hutchings [6].

The wear-regime map is a useful means of depicting the various regimes in which different modes of wear dominate. For steels sliding in air in the common pin-on-disc geometry, see Figure 1. Unlubricated sliding of most metals in air will fall under the general form even though the details of the map are specific for steels. The wear map is plotted with dimensionless variables. These variables are the normalized contact pressure (the normal load on the specimen pin divided by the nominal contact area times the indentation hardness of the softer material), and a normalized velocity (which is the sliding velocity divided by the velocity of heat flow).

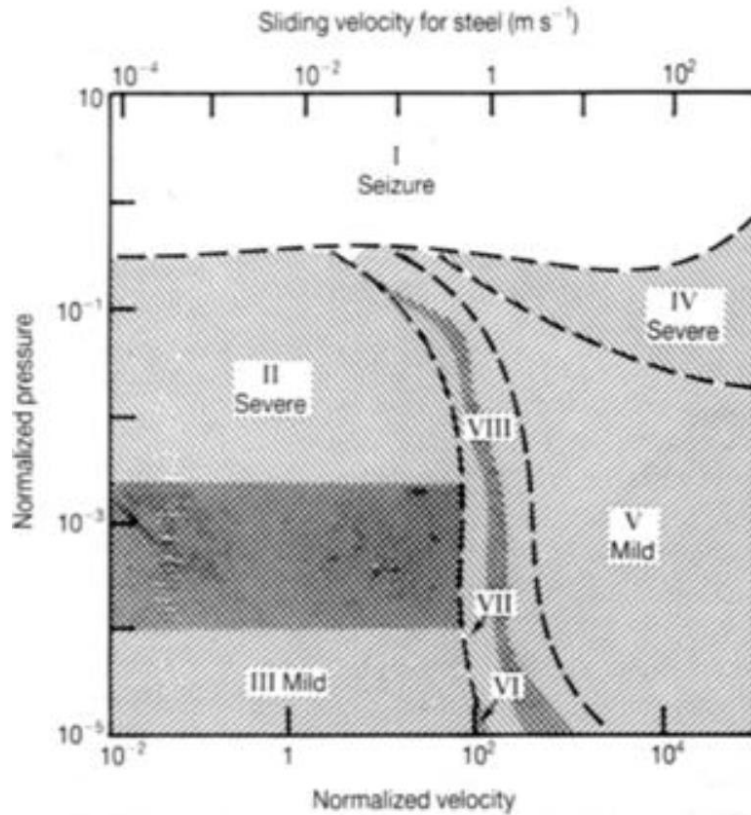


Figure 1: The wear-regime map for metals [6].

There are eight distinct regimes that can be identified in the wear-regime map. Regime I is associated with very high contact pressure where gross seizure of the surfaces occurs. This regime corresponds to the catastrophic growth of asperity junctions. The consequence is that the real area of contact becomes equal to the apparent area.

For regime II where relative low sliding velocities and high loads are occurring, the thin surface oxide film on the steel is penetrated at asperity contacts. This is a regime of severe wear which includes high surface tractions and the formation of metallic wear debris. Since the sliding velocity is low, the thermal effects are negligible.

In regime III the oxide is not being penetrated since there are lower loads compared to the II regime. Since the wear is mild there is formation of only oxide debris.

For regime IV high loads and sliding speeds are occurring. Since frictional power dissipation is high and thermal conduction is ineffective at removing heat from the interface, melting occurs. This regime incorporates high wear rate which lead to metal being removed as metallic droplets.

Regime V has low contact pressure but high sliding speed where the interface temperature is still high. The temperature is however below melting point which means that surface oxidation occurs rapidly. For this regime, the debris is oxide which consequently means that the wear is mild.

In regime VI local oxide growth is caused due to occurring hot-spots at asperity contacts. From this oxide layer the wear debris is spalling.

Metallic contact occurs at asperities for regime VII, which leads to severe wear through the formation of metallic debris.

For regime VIII, formation of martensite arises at the interface through local heating of asperities. This is followed by quenching through heat conduction into the bulk. Since martensite has a high strength it provides local mechanical support of the oxide film, which aids to reduce the amount of wear. Subsequently, the formation of oxide debris is the reason for wear to occur.

2.4 Delamination Wear

The delamination wear, or delaminative wear, is a wear type related to the adhesive wear mechanism that has large influence on the wheel and rail wear. This is the type of wear which has been specifically focused on when attempts for the simulation has been done. This subchapter is mainly based on *An overview of the delamination theory of wear* by Nam P. Suh [7].

There are five processes that are involved in delamination wear: transmission of forces, deformation, crack nucleation, crack propagation, and wear sheet separation. These sequential events which lead to wear particle formation for the delamination theory of wear are thoroughly described below. However, the events may be more independent if there are pre-existing subsurface cracks.

1. Via adhesive and plowing actions, the pressure and friction forces are transmitted through the contact points when two sliding surfaces come into contact. Softer surface asperities are easily deformed and some are even fractured by the repeated loading action. Either when these asperities are deformed or when they are removed, a relatively smooth surface is generated. The contact is not just an asperity-to-asperity contact once the surface becomes smooth. Now, the contact is rather an asperity-plane contact where each point along the softer surface experiences cyclic loading as the asperities of the harder surface plow it.
2. Plastic shear deformation is induced due to that the surface traction is utilized by the harder asperities on the softer surface. This plastic deformation accumulates with repeated loading.
3. As a result of the continuous subsurface deformation, cracks are nucleated below the surface. Because of a triaxial state of highly compressive stress that exists right below the contact regions, nucleation of cracks exceedingly close to the surface is not favoured.
4. Additional loading and deformation causes cracks to extend and propagate once they are present. This can lead to a network of cracks when the cracks are joining neighbouring ones. The cracks tend to propagate parallel to the surface at a depth that is governed by material properties and the coefficient of friction. The nucleation of the crack is the rate controlling mechanism in the case when cracks cannot propagate as a consequence of either limited deformation or a tangential traction at the asperity contact which is extremely small.

- At certain weak positions, the cracks finally shear to the surface and create long and thin *delaminating* wear sheets. The location of the subsurface crack growth controls the thickness of a wear sheet. Though, the subsurface crack growth is in turn governed by the pressure and friction forces at the surface.

To some extent the surfaces created by the delamination wear process, but mainly all machined surfaces, have asperities. In the occurrence of harder surfaces sliding over softer surfaces, the softer asperities either deform or fracture immediately. By the sliding process and the mechanism of removal, the rate at which these asperities are removed depend on the initial surface roughness, the applied load and the mechanical properties of the asperities.

Generation of wear particles occur when a subsurface crack breaks through to the surface. The crack reaches the surface after the asperity moves over the crack since the propagating end of the crack always is located behind the moving asperity. Here, the propagating end of the crack is usually the crack tip where the stress is maximal. As a result of this, the particle is elevated from the surface so that the underside of the wear particle is facing the direction opposite to the slider motion, see Figure 2. Compared to similar flat particles that are formed by the deformed asperities, this direction is opposite to that. Thus, this enables a distinction between particles formed by deformed asperities and from those formed by subsurface crack propagation.

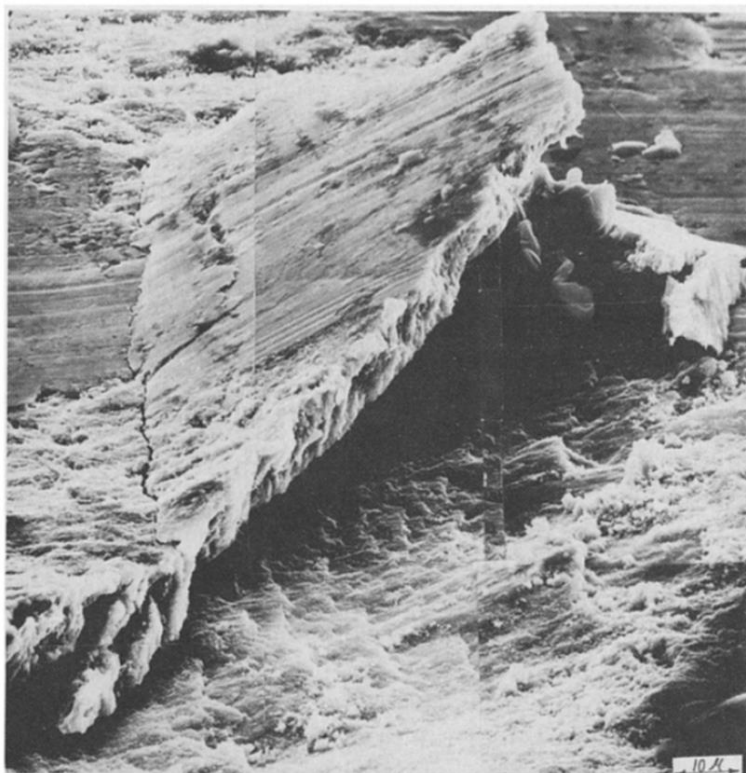


Figure 2: Wear sheet formation in an iron solid solution. The sheet is lifting up opposite to the sliding direction which in this figure is from right to left [7].

In the next chapter, the fundamentals of *contact mechanics* will be presented including Hertz theory along with the Hertzian line contact with rolling or sliding in full-slip.

3 Contact Mechanics

The area of contact mechanics is important to consider for both a wear phenomenon aspect as well as for a fracture mechanics point of view. Of especially great interest for a fracture mechanics aspect is the resulting shear stresses on and below the surface. Hence, this chapter contain an introduction to Hertz theory and its assumptions together with a subchapter about Hertzian line contact with rolling or sliding in full-slip. This contact mechanics chapter is mainly based on the information given by Hossein-Nia, *On Heavy-Haul Wheel Damages using Vehicle Dynamics Simulation* [4].

The researcher at the University of Berlin, Heinrich Hertz, published a paper called *On the contact of elastic solids* in 1882. This can be seen as the start of the knowledge of contact mechanics as the theory in Hertz's paper provides a closed-form solution to the normal contact problem. The assumptions that are the basis for the Hertz theory are:

- Displacements and strains are small.
- The bodies in contact are homogeneous, isotropic and linearly elastic.
- Smooth surfaces where the surface roughness is neglected (frictionless contact)
- The dimensions of the contact patch are significantly smaller than the dimensions of the bodies in contact. The dimensions of the patch are furthermore also smaller than the relative radii of the bodies in contact. Due to an assumption where the contact partners are semi-infinite bodies limited by a straight plane, the stresses can from this be approximately calculated. This is the so called half-space assumption.
- The curvature of the bodies in contact is constant.
- The materials of the bodies are quasi-identical.

The Hertz theory can often be used in many railway applications since the assumptions of the theory are here generally valid. Some of the assumptions could however be violated in a few cases. For instance, in case of high loads that are above the elastic shakedown and where some plastic flow could appear, linear elasticity is not valid. The size and shape of the patch is affected by this. Furthermore, where wheel and rail have a conformal contact, the half-space assumption is uncertain. This can occur due to wheel profile wear or flange contact.

3.1 Hertzian Line Contact in Full-Slip

For a cylinder with radius R that is rolling and/or sliding in full-slip condition over an elastic half space, the interface patch will be modelled as a line of contact with the half-length of a , see Figure 3. The normal pressure is then according to Hertz:

$$p(x) = \frac{2P}{\pi a^2} (a^2 - x^2)^{1/2} \quad (3.1)$$

where,

$$P = \frac{\pi a^2 E^*}{4R}, \quad E^* = \frac{E}{2(1 - \nu^2)} \quad \text{and} \quad p_0 = \frac{2P}{\pi a}$$

Here, E^* is the equivalent modulus of elasticity and p_0 the point of contact.

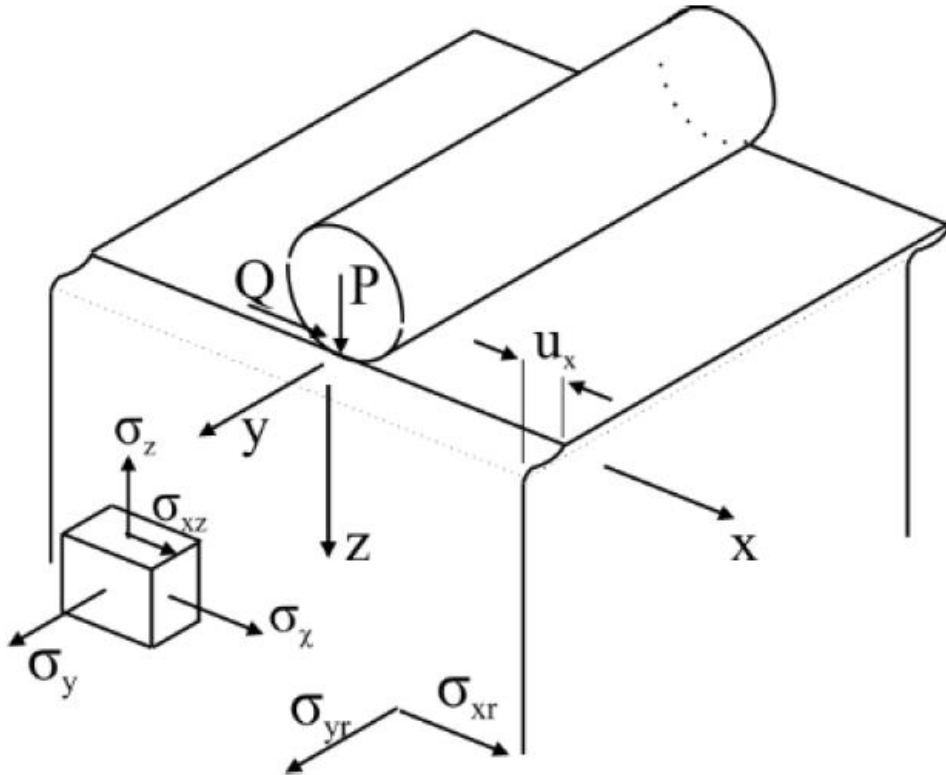


Figure 3: Cylinder in rolling-sliding contact with an elastic half-space [4].

The tangential traction, $q(x)$, will in the presence of friction be:

$$q(x) = \mp \frac{2\mu P}{\pi a^2} (a^2 - x^2)^{1/2} \quad (3.2)$$

As can be noted in the equation for the normal pressure is the similarity to the equation for the tangential traction where the only difference is the friction coefficient μ for the latter. When the stresses in longitudinal and vertical directions are retrieved along with the shear stress (which will not be derived here), the principal shear stress can be expressed as:

$$\tau_1 = \frac{1}{2} ((\sigma_x - \sigma_z)^2 + 4\tau_{xz}^2)^{1/2} \quad (3.3)$$

In Figure 4, the contours of the normalised principal shear stress τ_1/p_0 is visualised at surface and sub-surface under rolling with different friction coefficients. This is achieved with help from a Matlab script retrieved from Saeed Hossein-Nia where equation (3.3) is utilized. The friction coefficients range from $\mu = 0$ to $\mu = 0.5$ with an increment of 0.1 from top left to bottom right. For the case of $\mu = 0$ it can be seen that the maximum shear stress is located below the surface at $z = -0.79a$ where $x = 0$ is the symmetry line.

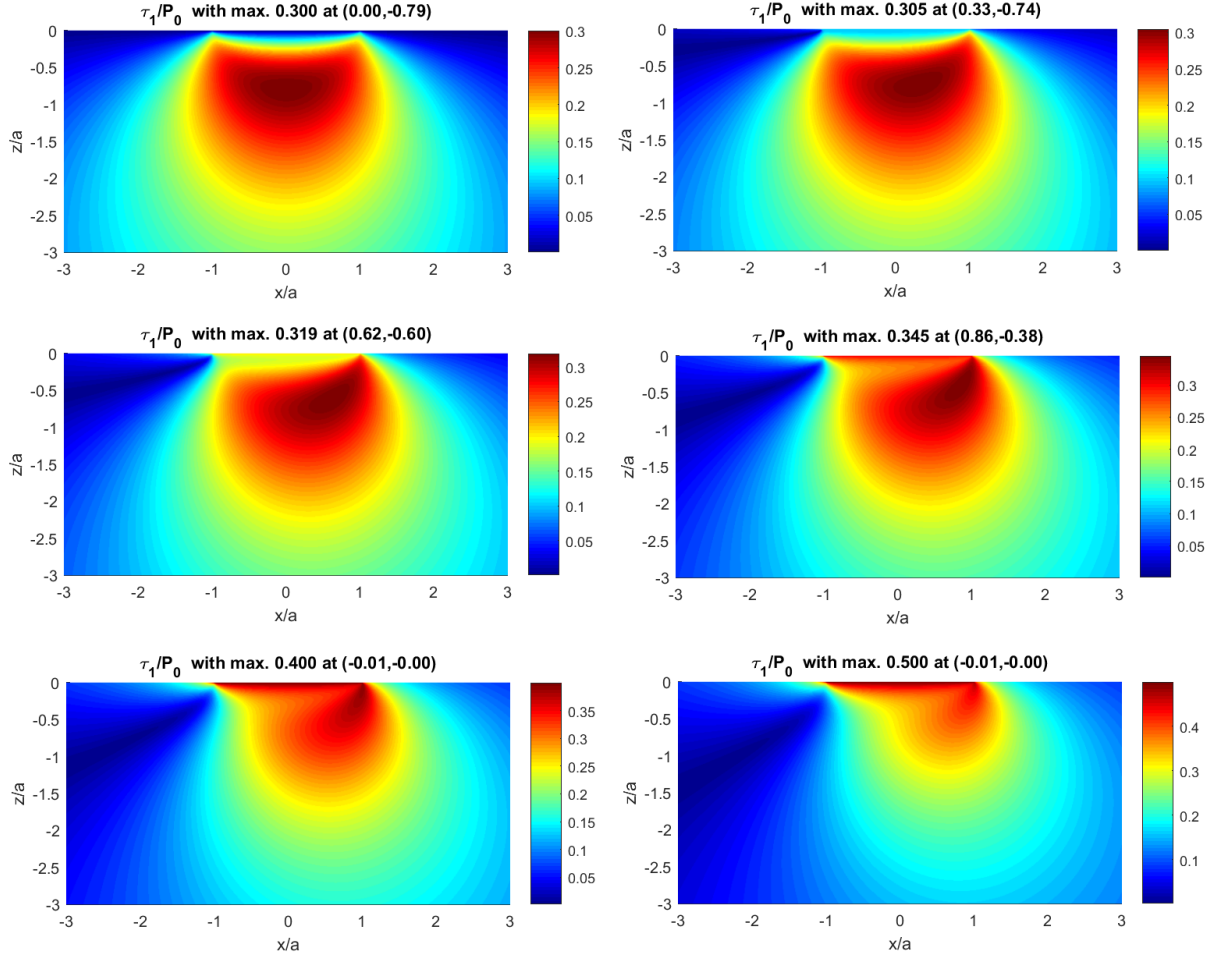


Figure 4: The normalised principal shear stress with $\mu = 0$ (top left), $\mu = 0.1$ (top right), $\mu = 0.2$ (middle left), $\mu = 0.3$ (middle right), $\mu = 0.4$ (bottom left), and $\mu = 0.5$ (bottom right).

Under a sliding contact however, the condition is different both at the surface and below the surface. Due to tangential traction $q(x)$, the longitudinal stress σ_x reaches its maximum compressive stress at the surface ($z = 0$) with the value $-2q_0$ at the leading edge of the contact area ($x = -a$). At the trailing edge ($x = a$), the maximum tension $2q_0$ is reached. The normal pressure applied at the surface leads to an equal stress at the surface. In Figure 5 the surface stresses due to the frictional traction $q(x)$ is visualized.

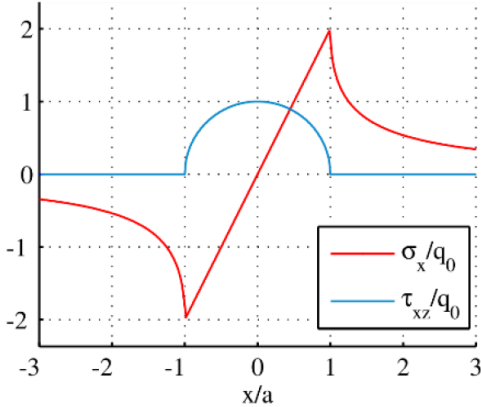


Figure 5: Surface stresses for sliding contact with friction [4].

An increased magnitude of the maximum principal shear stress occurs when the tangential traction $q(x)$ is increased. Moreover, higher friction values tend to move it closer to the surface. For example, the growth of the maximum value of the principal shear stress for the case with friction value $\mu = 0.1$ to the case with $\mu = 0.3$ is roughly 13%. This location moves towards the trailing edge ($x = a$) of the contact patch at the surface.

In the upcoming chapter, theory about *fracture mechanics* will be presented which specifically include crack initiation, the stress intensity approach, effect of specimen geometry, linear elastic fracture mechanics (LEFM), elasto-plastic fracture mechanics and extended finite element method (XFEM).

4 Fracture Mechanics

Failure due to fracture creates high costs and can lead to many casualties and injuries. There are many different reasons for which failures have occurred historically. Among these reasons include uncertainties in the loading or environment, inadequacies in design, deficiencies in construction or maintenance as well as defects in the materials. It is of great necessity to consider as many factors as possible that could lead to failure when life is at risk. The information provided in this chapter is predominantly based on *Introduction to Fracture Mechanics*, by David Roylance [8].

By manipulation of the microstructure so as to inhibit dislocation motion, the strength of structural metals like steel can be increased to very high levels. This unfortunately renders the material increasingly brittle. This can lead to the risks of cracks forming and propagating catastrophically with very little warning. Engineering disasters that are related directly to this phenomenon are an unfortunate number. Since there are procedures available that can safeguard against brittle fractures, engineers must be aware of these measures.

In high-strength materials the central difficulty in designing against fracture is that the local stresses can be modified by the presence of cracks to such an extent that the elastic stress analyses are insufficient even though the evaluation by the designers is carefully employed. A crack can propagate catastrophically through the structure when it reaches a certain critical length. This can occur even though the gross stress is much less than what would normally cause yield or failure in a tensile specimen. Fracture mechanics is the area of study which refers to a vital specialization within solid mechanics in which the presence of a crack is assumed. For the crack, one aspires to find some quantitative relations between its length and the material's inherent resistance to crack growth as well as the stress at which the crack propagates at high speed to cause structural failure.

4.1 Crack Initiation

Research around the initiation of fractures is extremely vital in the prevention of early failures in machine equipment, vehicles or its components. The safety aspects of evaluating the behaviour of crack initiation are quite indisputable. There is however additional incentives such as to increase the efficiency and reliability in for instance the train services while concurrently reducing the maintenance costs.

Nucleation of fractures is a complex process that is controlled both by the repartition of flaws in matter and by mechanical controls that make nuclei active or not, according to Davy et al. [9]. Here, flaws in matter can be pores, grain boundaries, cleavage planes, etc. The result of this is damage in the form of a micro crack that leads to the formation of faults or joints. The term *nuclei* can be used when describing the flaws that can be considered as growing cracks and the term *flaws* can be considered the imperfections in the material which has not been activated as of yet or grows considerably slower than cracks of the same characteristics. It seems that the main likely reason why nuclei forms is that it is related to stress redistribution by growing cracks, stress increase, thermal activation, chemical corrosion etc. There is a

feedback loop between the fracture nucleation and growth due to stress redistribution which can, depending on the initial distribution of weak and strong area defects, result in strikingly different geometries of the eventual fracture pattern.

Oliveira et al. [10] suggests that most of the studies of contact fracture have considered the behaviour of uncoated brittle solids where the analyses of fracture under sliding contact are of particular interest. Calculations show that cracks initiate at the surface immediately behind the contact where the tensile stress is the greatest when an indenter slides over the surface of a homogeneous solid. One usually observes an array of cracks in the wake of the indenter since several adjacent cracks might propagate in this way. The coefficient of sliding friction seems to be particularly significant for the fracture load. The fracture load is furthermore sensitive to the initial flaw size in the solid.

According to Spriestersbach et al. [11], cracks are often induced from so called non-metallic inclusions. An inclusion is any material that is trapped inside another material or just air bubbles inside a material. Around these inclusions the stresses tend to be much higher than in the rest of the material and this is one reason for the initiation of cracks in these regions. Fatigue properties in the high cycle fatigue regime are strongly affected by flaws inside the material like non-metallic inclusions.

There is a higher potency of crack initiation in materials where there is a case of serious property mismatching between matrix and defects. Also, higher strength materials seem to be more sensitive to soft inclusions, where the elastic modulus is lower than the matrix, as stated by Zhu et al. [12].

According to Ekberg [13], pores seem to be one of the most dangerous types of material imperfections in railway wheels and according to the theory of elasticity; the shape of the defect will have a major influence. In reality, it is however not certain that this influence is equally severe for the loaded component. This is because a defect will be entrenched in a smoothly shaped volume of plastically deformed material. According to the theory of plasticity, the defect size has no influence. The defect will nevertheless have an effect in reality where the estimation of the magnitude can be made using a model based on a criterion that was originally proposed by Murakami [14] [15].

4.2 The Stress Intensity Approach

Even though the energy-balance approach can provide some insights to the fracture process (study [8] for more information), an alternative method that examines the stress state near the tip of a sharp crack directly has in engineering practices been proven more useful. This method is called the stress intensity approach. It is common to treat three types of cracks in fracture mechanics that is termed as mode I, II, and III as visualised in Figure 6. Mode I is the tensile-opening mode and is especially emphasized in this section while mode II and III are different shear sliding modes; in-plane shear and out-of-plane shear respectively.

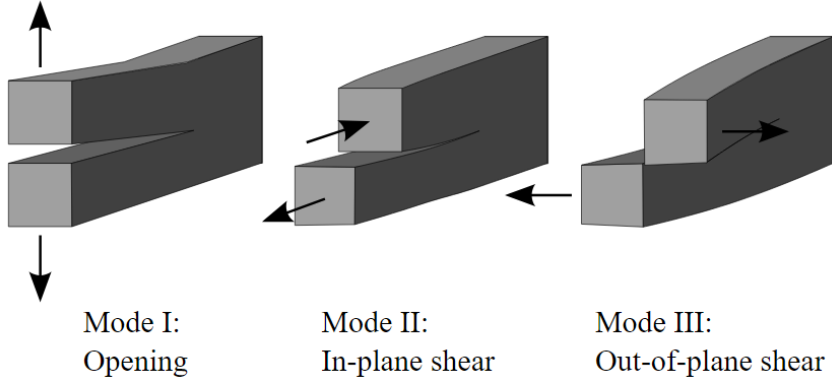


Figure 6: The three types of cracks in fracture mechanics are mode I (Opening), II (In-plane shear), and III (Out-of-plane shear) [16].

The opening-mode stress equations which are based on the semi-inverse method developed by Westergaard are shown below:

$$\sigma_x = \frac{K_I}{\sqrt{2\pi r}} \cos\left(\frac{\theta}{2}\right) \left\{ 1 - \sin\left(\frac{\theta}{2}\right) \sin\left(\frac{3\theta}{2}\right) \right\} + \dots \quad (4.1)$$

$$\sigma_y = \frac{K_I}{\sqrt{2\pi r}} \cos\left(\frac{\theta}{2}\right) \left\{ 1 + \sin\left(\frac{\theta}{2}\right) \sin\left(\frac{3\theta}{2}\right) \right\} + \dots \quad (4.2)$$

$$\tau_{xy} = \frac{K_I}{\sqrt{2\pi r}} \cos\left(\frac{\theta}{2}\right) \cos\left(\frac{3\theta}{2}\right) \sin\left(\frac{\theta}{2}\right) \dots \quad (4.3)$$

The second and higher order terms that are indicated by dots may be neglected for distances close to the crack tip ($r \leq 0.1a$). These relations cease to apply at large distances from the crack tip where the stresses approach their far-field values that would be obtained where the crack is not present. A very important parameter that is present in the equations above is the *stress intensity factor* (SIF), K_I . Here, the subscript I refer to the crack opening mode. However, similar relations apply in the modes II and III. Three factors are shown in the equations that taken together depict the stress near the crack tip; the denominator factor $(2\pi r)^{-1/2}$ acts as the stress distribution's singular nature; σ is approaching infinity as the crack tip is approached, with a dependency of $r^{-1/2}$. The angular dependency is separable as another factor; e.g. $f_x = \cos\left(\frac{\theta}{2}\right) \left(1 - \sin\left(\frac{\theta}{2}\right) \sin\left(\frac{3\theta}{2}\right) \right) + \dots$. The stress intensity factor, K_I , contains the dependence on applied stress σ_∞ , the specimen geometry, and the crack length a . It gives the overall intensity of the stress distribution, henceforth its name.

In a large sheet for the specific case of a central crack of width $2a$ or and edge crack of length $2a$, the SIF can be expressed as:

$$K_I = \sigma_\infty \sqrt{\pi a} \quad (4.4)$$

For an edge crack of length a in the edge of a large sheet the SIF can be expressed as:

$$K_I = 1.12\sigma_\infty\sqrt{\pi a} \quad (4.5)$$

In Table 1, some expressions for K_I for some several geometries are given.

Table 1: Stress intensity factors for different types of cracks and common geometries [8].

Type of Crack	Stress Intensity Factor, K_I
Center crack, length $2a$, in an infinite plate	$\sigma_\infty\sqrt{\pi a}$
Edge crack, length a , in a semi-infinite plate	$1.12 \sigma_\infty\sqrt{\pi a}$
Central penny-shaped crack, radius a , in in infinite body	$2 \sigma_\infty\sqrt{\frac{a}{\pi}}$
Center crack, length $2a$ in plate of width W	$\sigma_\infty\sqrt{W \tan(\frac{\pi a}{W})}$
2 symmetrical edge cracks, each length a , in plate of total width W	$\sigma_\infty\sqrt{W \left[\tan\left(\frac{\pi a}{W}\right) + 0.1 \sin\left(\frac{2\pi a}{W}\right) \right]}$

It is in the design and analysis that the SIFs are used by arguing that the material can withstand crack tip stresses up to a critical value of stress intensity that is termed K_{Ic} . Beyond this critical value of stress intensity, the crack propagates rapidly. This *critical stress intensity factor* can then be explained as being a measure of material toughness. Related to the crack length a , and the fracture toughness is the failure stress σ_f which is expressed as:

$$\sigma_f = \frac{K_{Ic}}{\alpha\sqrt{\pi a}} \quad (4.6)$$

where the geometrical parameter α is equal to 1 for edge cracks and for other situations it is generally on the order of unity. For a wide variety of specimen and crack geometries there are tabulated expressions for α and for new situations the finite element methods are available to compute it.

The stress intensity and energy viewpoints are interrelated and for in plane stress the relation is:

$$\sigma_f = \sqrt{\frac{EG_c}{\pi a}} = \frac{K_{Ic}}{\sqrt{\pi a}} \Rightarrow K_{Ic}^2 = EG_c \quad (4.7)$$

For plane strain the relation can be expressed as:

$$K_{Ic}^2 = EG_c(1 - \nu^2) \quad (4.8)$$

Metals with Poisson's ratio of $\nu = 0.3$ give the factor $(1 - \nu^2) = 0.91$ which is not a big change. The numerical values of G_c and K_{Ic} are however very different from each other in plane stress and plane strain situations.

The fracture toughness G_c and K_{Ic} for various materials is listed in Table 2. It can be noticed that they vary over a wide range from material to material. Among the most common materials, steel alloys are the best regarding absolute resistance to crack propagation. However, when rated on a per-pound base, some polymers can be very tough as well.

Table 2: Fracture toughness of different materials [8].

Material	G_{Ic} (kJm ⁻²)	K_{Ic} (MNm ²)	E (GPa)
Steel alloy	107	150	210
Aluminum alloy	20	37	69
Polyethylene	20 (J_{Ic})	—	0.15
High-impact polystyrene	15.8 (J_{Ic})	—	2.1
Steel — mild	12	50	210
Rubber	13	—	0.001
Glass-reinforced thermoset	7	7	7
Rubber-toughened epoxy	2	2.2	2.4
PMMA	0.5	1.1	2.5
Polystyrene	0.4	1.1	3
Wood	0.12	0.5	2.1
Glass	0.007	0.7	70

4.3 Effect of Specimen Geometry

The material toughness, or in other words the resistance to crack growth in a material, is governed by the energy absorbed as the crack moves forward. This energy is, for an exceptionally brittle material like window glass, primarily just that of rupturing the chemical bonds along the plane of the crack. By far the largest part of the fracture energy is being associated with plastic flow near the crack tip. Yet, in regards of resistance to crack growth, bond rupture plays a relatively small role in tougher materials. There is a plastic zone near the crack tip of which the predicted stresses from equation (4.1-4.3) would be above the material's yield stress σ_y . Since the stress can't rise above σ_y , the stress in the crack tip zone

are actually σ_y rather than what was given in equation (4.1-4.3). By using equations (4.1-4.3), the distance r_p this zone extends along the x-axis can be found. With $\theta = 0$, the distance at which the crack tip stress reduces to σ_Y is retrieved as:

$$\sigma_y = \sigma_Y = \frac{K_I}{\sqrt{2\pi r_p}} \quad (4.9)$$

where,

$$r_p = \frac{K_I^2}{2\pi\sigma_Y^2}$$

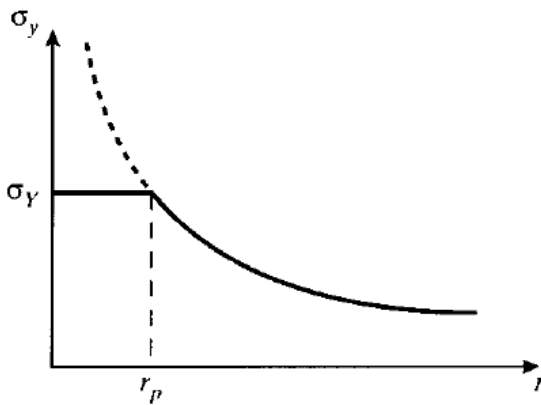


Figure 7: Yield is the limiting factor of the stress within zone r_p [8].

In Figure 7, this relation is demonstrated. The plastic zone size will increase when the stress intensity is increased, either by raising the imposed stress or by crack lengthening. However, the material's molecular or microstructural mobility is what the extent of the plastic flow is ultimately limited by. This means that the zone can become only so large. Unstable propagation follows when the zone can grow no larger and therefore the crack can no longer be constrained. It can be considered that the value of K_I , at which this occurs, is a material property named K_{Ic} .

The plastic zone size should not be too large as to interact with the specimen's free boundaries or to destroy the rudimentary nature of the singular stress distribution in order for the measured value of K_{Ic} to be valid. The specimen geometry for the ASTM specification for fracture toughness testing [17] is specified to insure that the specimen is large compared to the crack length and the plastic zone size:

$$a, B, (W - a) \geq 2.5 \left(\frac{K_I}{\sigma_Y} \right)^2 \quad (4.10)$$

where a is the crack length, B is the breadth and W is the depth of the specimen. It can be impossible to satisfy the above criteria in the case of when enough ductility exists. The view of the stress intensity must in these cases be abandoned in favour of alternative techniques such as the J-integral or the crack tip displacement (CTD) method (see subchapter 4.5 *Elasto-plastic fracture mechanics (EPFM)* for further information).

Essentially, the measured fracture toughness K_c or G_c is a measure of the extent of plastic deformation that is associated with crack propagation. When reducing the thickness of the specimen in half, it will naturally cut the volume of plastically deformed material roughly in half as well, and thus it is expected that the quantity of plastic flow scale linearly with the specimen thickness. Consequently, the toughness rises linearly initially with the specimen thickness as can be seen in Figure 8. What can also be seen is that eventually the toughness reaches a maximum which is followed up with a fall to a lower value. The toughness reaches a maximum at the critical thickness, t^* . The loss of toughness beyond this value is extremely important in the design against fracture since unrealistically optimistic values for G_c is yielded when using too thin of a specimen in measuring toughness. For valid fracture toughness testing, the specimen size requirements are such that the most conservative value is measured.

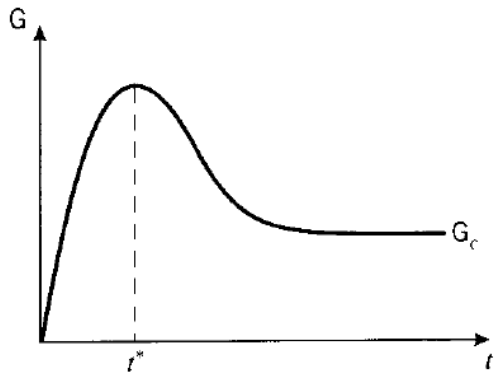


Figure 8: The influence of specimen thickness on toughness [8].

It is the critical thickness that causes the specimen to be dominated by a state of *plane strain*, as opposed to *plane stress*. Since no traction is applied at the sides of the specimen the stress in the through-thickness z direction must become zero. Furthermore, the stress will not have room to rise to considerable values within the material for a thin specimen. The specimen will experience a Poisson contraction that is given by $\varepsilon_z = \nu(\sigma_x + \sigma_y)$ and the strain in the z direction is not zero. However, material near the centre will be unable to contract laterally when the specimen is thicker which is due to the constraint of adjacent material. As the material now tries to contract but is prevented from doing so, the z -direction strain is zero and thus a tensile stress will ascend. At the outer surface the value of σ_z rises from zero where it reaches a maximum value that is given by $\sigma_z \approx \nu(\sigma_x + \sigma_y)$ at the critical thickness t^* as shown in Figure 9. It is important that the specimen thickness t must be such that $t \gg 2t^*$ in order to guarantee that the plane strain conditions will dominate.

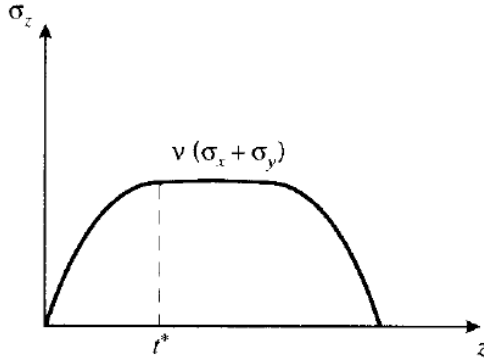


Figure 9: Transverse stress at crack tip [8].

4.4 Linear Elastic Fracture Mechanics (LEFM)

The local stresses in the vicinity of a crack tip are analysed according to the theory of elasticity in linear elastic fracture mechanics. The stress field around the crack tip will exhibit a singularity if the tip is considered to be infinitely sharp. This singularity can be quantified by the stress intensity factor, K . The prediction of crack propagation can be done with Paris' law that includes, among other variables, the range of stress intensity factor during a load cycle, ΔK :

$$\frac{da}{dN} = C(\Delta K)^m \quad (4.11)$$

Here, da/dN is the crack growth per load cycle while C and m are material parameters. In order for the LEFM to be valid, the crack length must be large compared to the plastic zone size. Materials that sustain large zones of plasticity or other type of damage before failure will violate the small-scale yielding criterion [13].

4.5 Elasto-Plastic Fracture Mechanics (EPFM)

The stress intensity factors can only be used for quantifying the state of stress in the vicinity of the crack tip as long as the plastic zone of the crack tip is regarded as small compared to the distinguishing dimensions of the crack. Other measures for the local state of stress at the crack tip needs to be implemented when this is no longer the case. One of these measures are the J -integral which allow for a larger plastic zone but at the same time carries the limitation of which strains are assumed to be small. Since the J -integral is an energy measure it will always be positive and therefore this may lead to predicaments when defining stress cycles in fatigue analysis. Also, since the J -integral was originally intended for non-linear elastic behaviour, one must take special care. For instance, one needs to take precaution in studies of which elasto-plastic loading is followed by elastic unloading. The fatigue impact can similarly be assumed to relate to the relative displacement of certain material points across the crack and adjacent to the crack tip. Crack tip displacement (CTD) is the title for this measure. One

of the main drawbacks with this approach is that it will be a challenge to define the *CTD* in a distinctive manner [13].

4.6 Extended Finite Element Method (XFEM)

This subchapter is mainly based on the paper *Crack growth simulation of stiffened fuselage panels using XFEM techniques* by Krishna Lok Singh, Kamal Keswani and Mallikarjun Vaggar [21].

When dealing with continuous field problems the standard finite element method (FEM) provides substantial advantages. It is however computationally expensive to retrieve accurate solutions with polynomial approximations for discontinuous field problems. When treating problems with evolving discontinuities, difficulties occur with mesh alignment with discontinuity since the mesh needs to be regenerated at each step. Furthermore, the singularity of the crack tip needs to be accurately represented by the approximation. The standard finite element methods are based on the piecewise differentiable polynomial approximations. Therefore, these methods are not well suited to problems with discontinuous rendering singular solutions. In non-homogeneous materials the order of singularity of stress field near a crack tip is same as that of the homogeneous materials. As the crack grows, there is a significant need to re-mesh or mesh in order for it to conform to the features provided in the traditional finite element methods. The introduction of the extended finite element method (XFEM) is an answer to the deficiency of the standard finite element methods in this regard and was created by Belytschko and Black [18].

The XFEM was developed to ease the difficulties in solving problems with localized features that by mesh refinement are not efficiently resolved. Hence, the XFEM is used extensively in many fields such as composites and fracture mechanics. To allow the presence of discontinuities in an element, the method enriches degrees of freedom with special displacement functions. The XFEM approximation is comprised of standard finite elements and enriched elements. The standard finite elements are used in the major part of the domain whereas the enriched elements are used in the enriched sub-domain. The enriched elements are applied in order to capture special solution properties like discontinuities and singularities. The main reason for adding enriched elements is to be able to expand the approximation space function of standard FEM that consequently gives a more accurate solution closer to the reality for the enriched approximation. XFEM is a very effective and versatile method to simulate initiation and growth of a discrete crack along a definite path in contrast to finite elements where continuous re-meshing is required.

The shape functions at node i can be denoted by $N_i(x)$ and the corresponding nodal displacement values of the dependent variable by u_i . For the approximation of the standard XFEM, a term for the standard finite element is used together with an enriched term that can capture discontinuous characteristics (heavy-side functions, crack tip singularity) in the domain k . The standard XFEM approximation $u(x)$ can be expressed as:

$$u_{xfem}(x) = \sum_{i \in k} N_i(x) u_i + \sum_{i \in k^*} N_i^*(x) b_i(x) a_i \quad (4.12)$$

Where the classical standard finite element part is represented by the first term and the enrichments based on the idea of the partition of unity approach is represented by the second term. Here, k^* is the set of the enriched nodes, u_i is the unknown displacement of the standard FEM at node i , a_i is the unknown enrichment at node i and $b_i(x)$ is the local enrichment function of node i . Any enrichment function $b_i(x)$ holds

$$\sum_{i \in k} [N_i(x) b_i(x)] = b_i(x) \quad (4.13)$$

based on the idea of the partition of unity. For capturing discontinuous characteristics in the domain, the discontinuous function $b_i(x)$ is utilized. The major key property of the standard XFEM is that any function $b_i(x)$ can be reproduced in the domain by local basis function $N_i(x)b_i(x)$ in order to solve discontinuous problems.

The representation of the crack away from the tip can be simplified by the Heaviside enrichment function, which is given by Jiang and Ying [19]. Two enrichment functions are generally incorporated into the XFEM displacement approximation in order to represent a crack. To represent the crack away from the tip, a Heaviside step function is used whereas for representation of the crack tip asymptotic displacement field, a more complex set of functions is utilized. The Heaviside step function can be expressed as:

$$H(x) = \begin{cases} 1, & \text{above crack} \\ -1, & \text{below crack} \end{cases} \quad (4.14)$$

This enrichment given by the Heaviside step function introduces a discontinuity in displacement across the crack. Four enrichment functions are given below for a linear elastic crack tip. These are used to incorporate the crack tip displacement field into elements containing the crack tip. From the asymptotic displacement field below, the crack-tip enrichment functions can be obtained:

$$a_i(r, \theta) = \begin{pmatrix} \sqrt{r} \sin\left(\frac{\theta}{2}\right) & \sqrt{r} \cos\left(\frac{\theta}{2}\right) \\ \sqrt{r} \sin\left(\frac{\theta}{2}\right) \sin\theta & \sqrt{r} \cos\left(\frac{\theta}{2}\right) \sin\theta \end{pmatrix} \quad (4.15)$$

Here, θ and r are the polar coordinates in the local crack tip coordinate system. The crack tip works as the origin and $\theta = 0$ is parallel to the crack. The first enrichment function acts as the Heaviside enrichment due to being discontinuous across the crack behind the tip in the element containing the crack tip. An example of a node being enriched by both the Heaviside function and crack tip enrichment features can be seen in Figure 10.

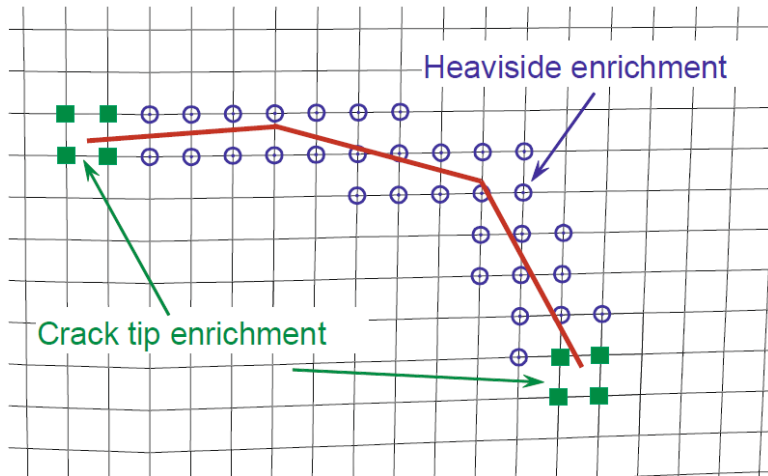


Figure 10: Enrichments in the XFEM. Circles: nodes with 2 additional DOFs. Squares: nodes with 8 additional DOFs [20].

A very important parameter for estimating the severity of a crack in cracked structures is the stress intensity factor. In case of an edge-cracked rectangular plate under tensile loading, the analytical solution for the stress intensity factor (SIF) is given by:

$$K_I = \sigma \sqrt{\pi a} F\left(\frac{a}{W}\right) \quad (4.16)$$

The upcoming chapter *FE-modelling* is about the pre-processing of the fracture propagation models. Here, the construction of the models is made where for instance the mesh, boundary conditions, pressure distribution and traction is defined.

5 FE-Modelling

The main objective with the thesis has been to create one or several fracture propagation models that can be utilized to predict crack growth and in the long run predict the failure of the material. This chapter is therefore dedicated to describe the most essential and relevant processes of designing the models in Abaqus together with clarifications of certain physical properties. The results will be presented in the results and discussion chapter in addition to analyses and interpretations of the results. The conclusions are gathered in the chapter with the same name.

The simulation is done through Abaqus which is a software suite that was originally released in 1978 and is used for its finite element analyses and computer-aided engineering. The product suite that is used in this work is the Abaqus/CAE which is a software application that can be used for both the modelling and analysis of mechanical components and assemblies (pre-processing) and visualising the finite element analysis result (post-processing) [22].

It is important to mention that the damage initiation criterion and the pressure distribution among other settings selected in Abaqus are not necessarily realistic values. Many different settings and values have been tested (not all presented here though) for the main reason of enhancing the understanding of different kinds of phenomena.

Before the simulation process can be explained, some simplifications and assumptions made needs to be mentioned first. Firstly, when surface traction is applied apart from the pressure distribution, sliding in full-slip is assumed. Only the tread is considered as the wheel contact and it can be perceived as the interface of the models are visualised upside-down (since it's the wheel that is simulated, not the rail). The location of the wheel-rail contact stresses is the same for every load cycle. For real circumstances though, the distribution of the pressure would differ depending on the time period of which a certain section of the wheel is in contact. For instance, the distribution would be different if the contact is in the beginning, middle or end, and you could say that the load is moving on the contact patch.

A Matlab-script has been received from Saeed Hossein-Nia in order to understand where the maximum principal shear stress is located (as can be read in chapter 3 about contact mechanics). Therefore, the inclusion has been placed at the maximum principal shear stress location for the case when the friction coefficient is $\mu = 0$. This is done in order to increase the chance of crack initiation and propagation. However, when the friction force is applied and increased, even though the maximum principal shear stress will be shifted towards the surface, the location of the inclusion has still been placed at the same point due to time restrictions.

The fracture mechanics method used in Abaqus is XFEM, as mentioned and thoroughly explained in the fracture mechanics chapter. Within the XFEM framework there are two different approaches; the *cohesive segment* approach and the *LEFM-based* approach. The cohesive segment approach follows the general framework for surface based cohesive

behaviour. It uses traction-separation laws and the damage properties are specified as part of the bulk material definition. This is the approach used in this work. The LEFM-based approach uses the *virtual crack closure technique*, VCCT, where the damage properties are specified via an interaction property assigned to the XFEM crack. There is an option in the interaction module in Abaqus that allow for selection of crack location. If this is not selected, the crack initiates automatically wherever certain damage initiation criteria in the traction-separation laws are exceeded. Automatic crack growth has been selected here for the two different models. The type of damage can for instance be defined as maximum principal strain or stress. The latter type of damage is used for all the models.

5.1 2D Model

The first model was designed in two dimensions with a so called *2D deformable shell* element for the sake of simplicity. Even though the depth dimension is neglected here, it can still give some indications of some fracture phenomena (for more details, see chapter 4.3 about the effect of specimen geometry). The precision of the results (stresses, crack extension, etc.) depend on the resolution of the mesh. A fine mesh gives for instance often higher and more precise stress distribution in the model. The downside with a fine mesh is that it is more computationally expensive. The mesh element type used for this two-dimensional model is called CPS4R and is a 4-node bilinear plane stress quadrilateral type of element with reduced integration and hourglass control. The number of elements used in the model is 39351. The mesh for the whole plate model is shown in Figure 11.

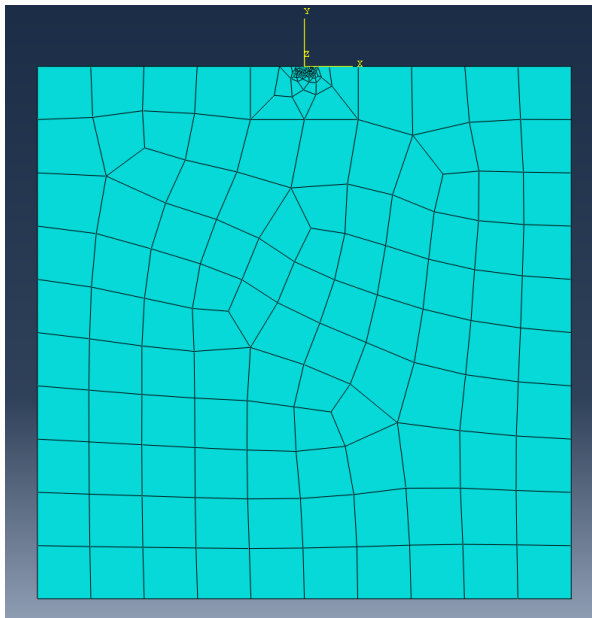


Figure 11: The mesh distribution for the 2D model.

One can notice that the mesh resolution is quite coarse away from the placed circle inclusion below the origin of the coordinate system. Yet, it has been designed in a way so that the closer one gets to the inclusion, the finer the mesh, as can be seen in Figure 12. This is deliberately

designed this way since the areas around the inclusion are the most vital regions in the study of fracture.

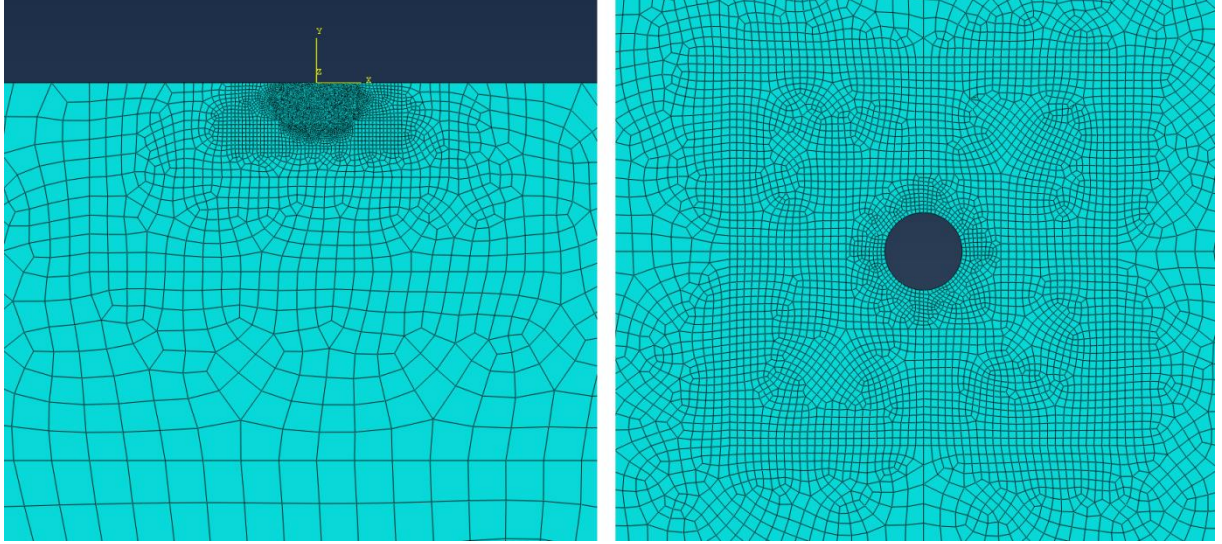


Figure 12: Finer mesh closer to the inclusion.

Non-linear geometry is activated in order to achieve higher accuracy since the strains can be quite substantial around the surface area of contact and around the inclusion. The material properties for this model are, $E = 2.06 \text{ GPa}$, $\nu = 0.3$, and $\text{maxps} = 120 \text{ Pa}$. The maxps value is the maximum principal stress that an element needs to exceed in order for a crack to nucleate and/or propagate. The radius of the inclusion is in this model $r = 0.05 \text{ mm}$, the contact radius is $a = 8.7 \text{ mm}$ and the inclusion is placed in a depth of $y = -0.79a$. This is the depth of which the principal shear stresses are maximum in the case of $\mu = 0$, for the Hertzian theory of line contact. The pressure distribution applied at the surface contact is equal to equation (3.1), where $P = 200 \text{ Pa}$ and x is defined on the interval: $-8.7 \leq x \leq 8.7 \text{ mm}$. The traction is directed to the left and applied in the surface contact that is equal to equation (3.2). Both the pressure distribution and the traction can be seen applied in the model in Figure 13. The amplitude chosen for the simulation is shown in Figure 14 and is comprised of 5 peaks. The boundary conditions are defined as being free in y -direction, with all the other DOFs fixed for the two top corners. For the two bottom corners, all the DOFs are fixed.

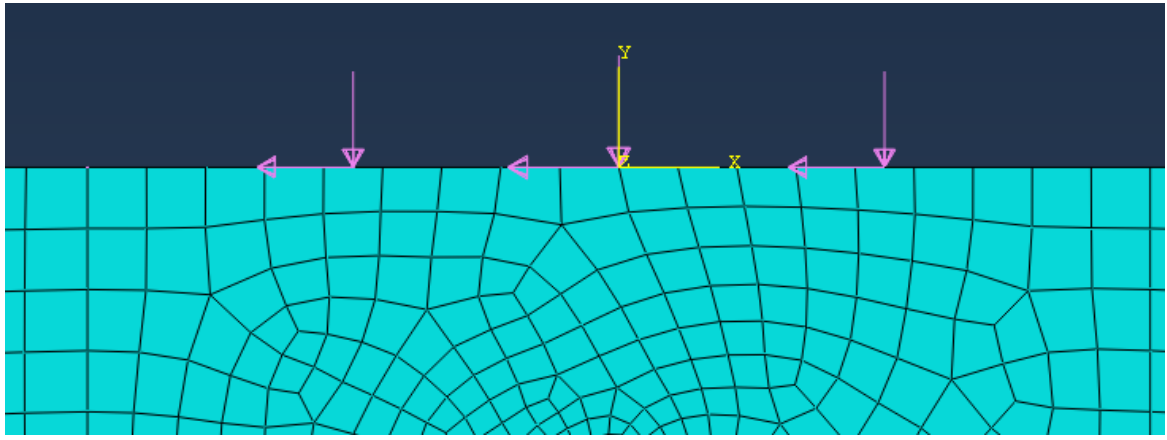


Figure 13: The pressure distribution and traction applied at the contact surface.

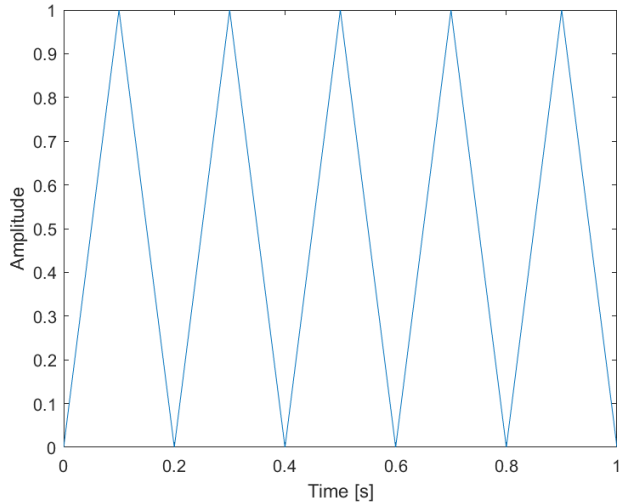


Figure 14: Amplitude function used in order to simulate 5 cycles.

5.2 3D Model

The thin three-dimensional model is created with certain fracture mechanics theories in mind. Especially the effect the thickness of the block model has on the fracture toughness, see chapter 4.3 *Effect of specimen geometry*. This applies however mainly when plasticity is considered. Consequently, material properties that consider plastic behaviour can conveniently be implemented in the future.

This model's material properties are also $E = 2.06 \text{ GPa}$, $\nu = 0.3$ and $\text{maxps} = 120 \text{ Pa}$. The radius of the inclusion is in this model larger with $r = 0.6 \text{ mm}$, the contact radius is $a = 10 \text{ mm}$ and the cylinder inclusion is placed in a depth of $y = -0.79a$. The pressure distribution applied at the surface contact is equal to the equation (3.1), where $P = 55 \text{ Pa}$ and x is defined on the interval: $-10 \leq x \leq 10 \text{ mm}$. The traction applied in the surface contact is equal to equation (3.2). The thickness of the model is 2 mm. Both the pressure distribution and the traction are for this 3D model constant in the z -direction (the through-thickness direction) for the reason of simplifying the problem. The number of elements used in the

model is 17888. The mesh around the inclusion is shown in Figure 15. The pressure distribution and traction are presented in Figure 16.

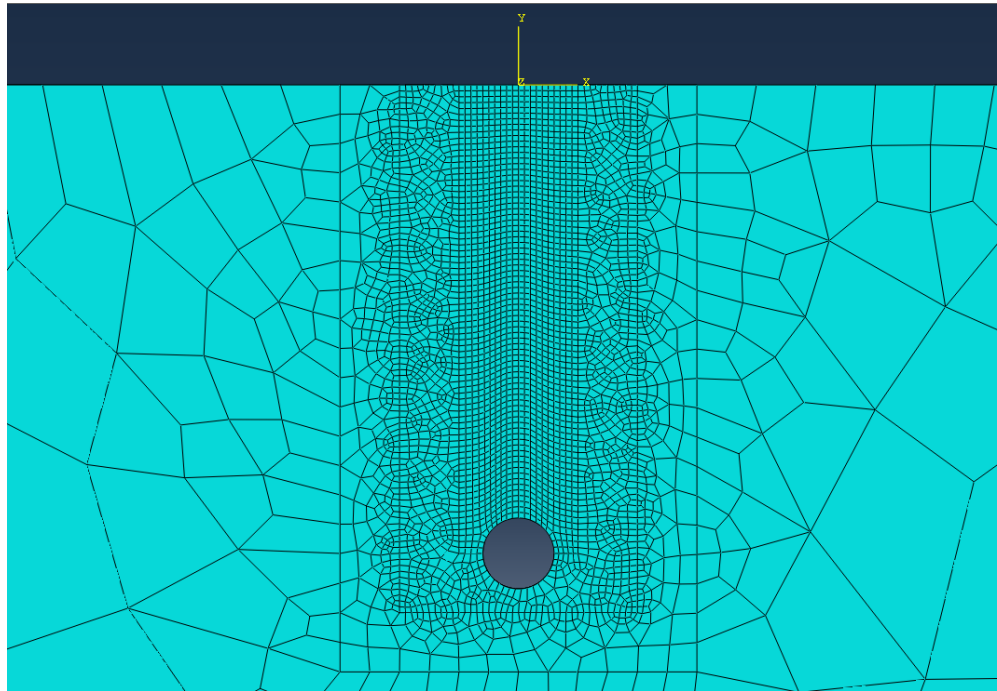


Figure 15: The mesh for the 3D model near the inclusion.

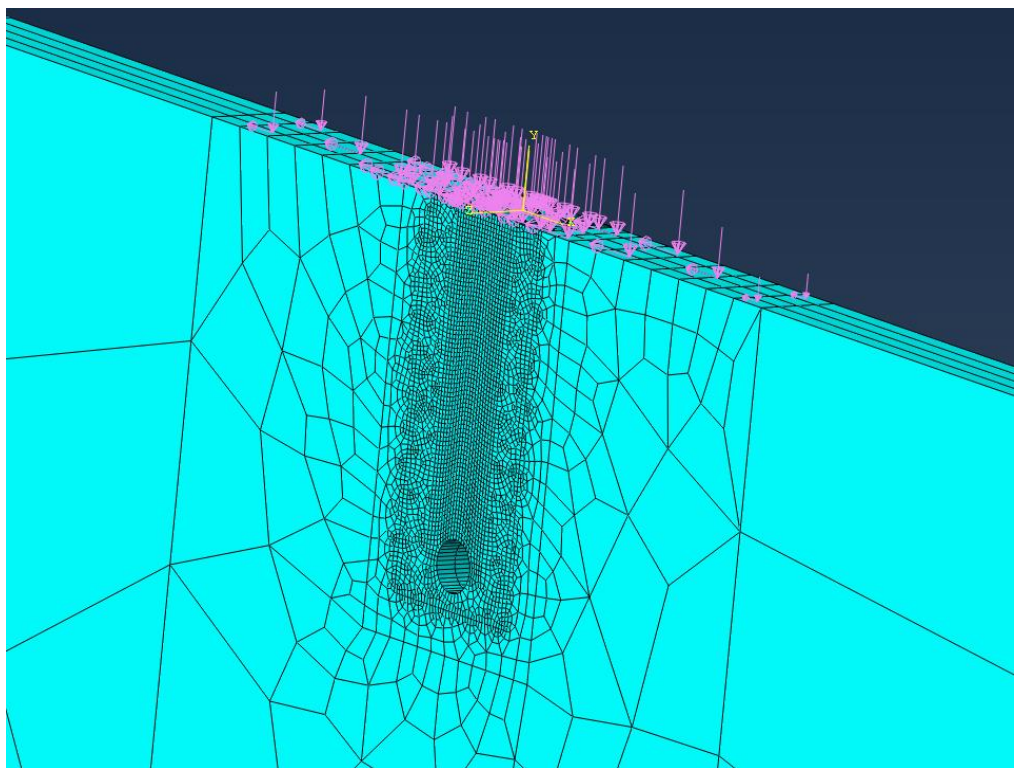


Figure 16: The pressure distribution and traction for the 3D model.

The next chapter visualises the results of the simulations along with interpretations of them.

6 Results and Discussions

Here follows the results for both the 2D and 3D model in regards to the Von Mises stress, different tensile stresses, and crack propagation below the surface around the inclusion and at the surface. The main focus of this chapter has been directed towards the 2D model.

Discussions and interpretations that are more general and revolve around both the 2D and 3D model will be concentrated in chapter 6.3 *General*.

6.1 2D Model

The Von Mises stress distribution around the inclusion are shown in Figure 17, for a friction coefficient of $\mu = 0$. The stress near to the contact surface is approximately half of what the maximum is and this maximum is retrieved at the sides of the inclusion.

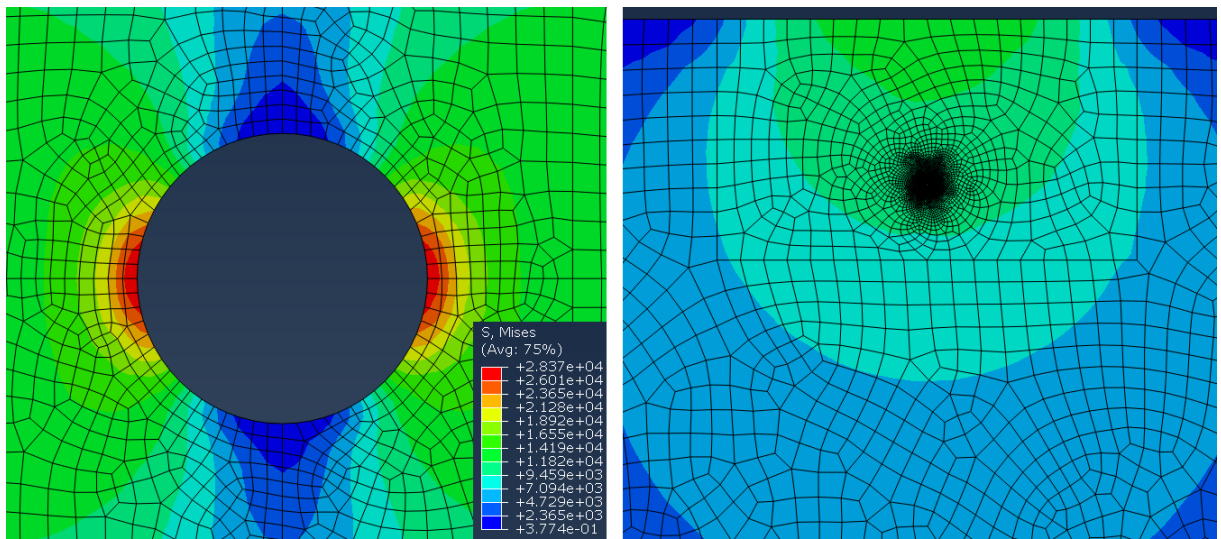


Figure 17: The Von Mises stress distribution around the inclusion for $\mu = 0$ (no traction applied).

It seems though that the cracks are nucleating at the top of the inclusion for low friction coefficients of 0.2 and below. This occurs even though the highest Von Mises stress is located at the sides of the inclusion. This is because the maximum stress at the sides of the inclusion is compressive stresses, and therefore a fracture is not able to open up. However, because of tensile stresses at the top of the inclusion, fractures tend to extend, as can be seen in Figure 18 and 19 for the σ_{xx} and σ_{yy} stresses respectively. In these figures, the stresses are shown near the inclusion as well as on the surface above the inclusion for three different friction values. It can be seen that the maximum positive value for σ_{xx} and σ_{yy} is located at the top and bottom of the inclusion and σ_{xx} is higher for the three tested friction values. This means that there is a strong tensile stress that tends to open up the fracture. The maximum negative value for σ_{xx} is located at the contact patch surface whereas it is located at the sides of the inclusion for the σ_{yy} . This signifies that there are compressive stresses near the surface in the longitudinal direction and that the sides of the inclusion are exposed to compressive stresses in the vertical direction.

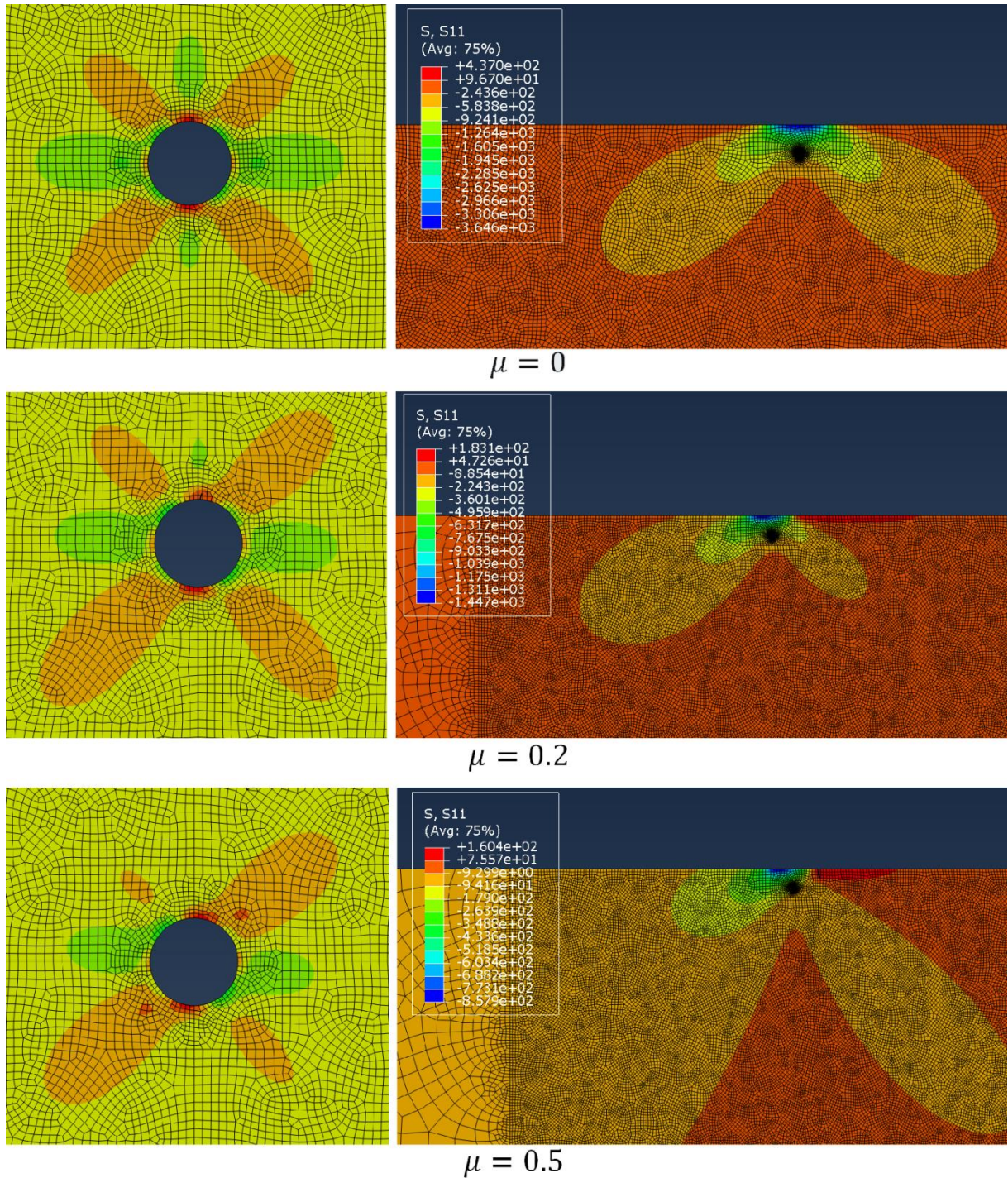


Figure 18: The σ_{xx} stress distribution for different friction values.

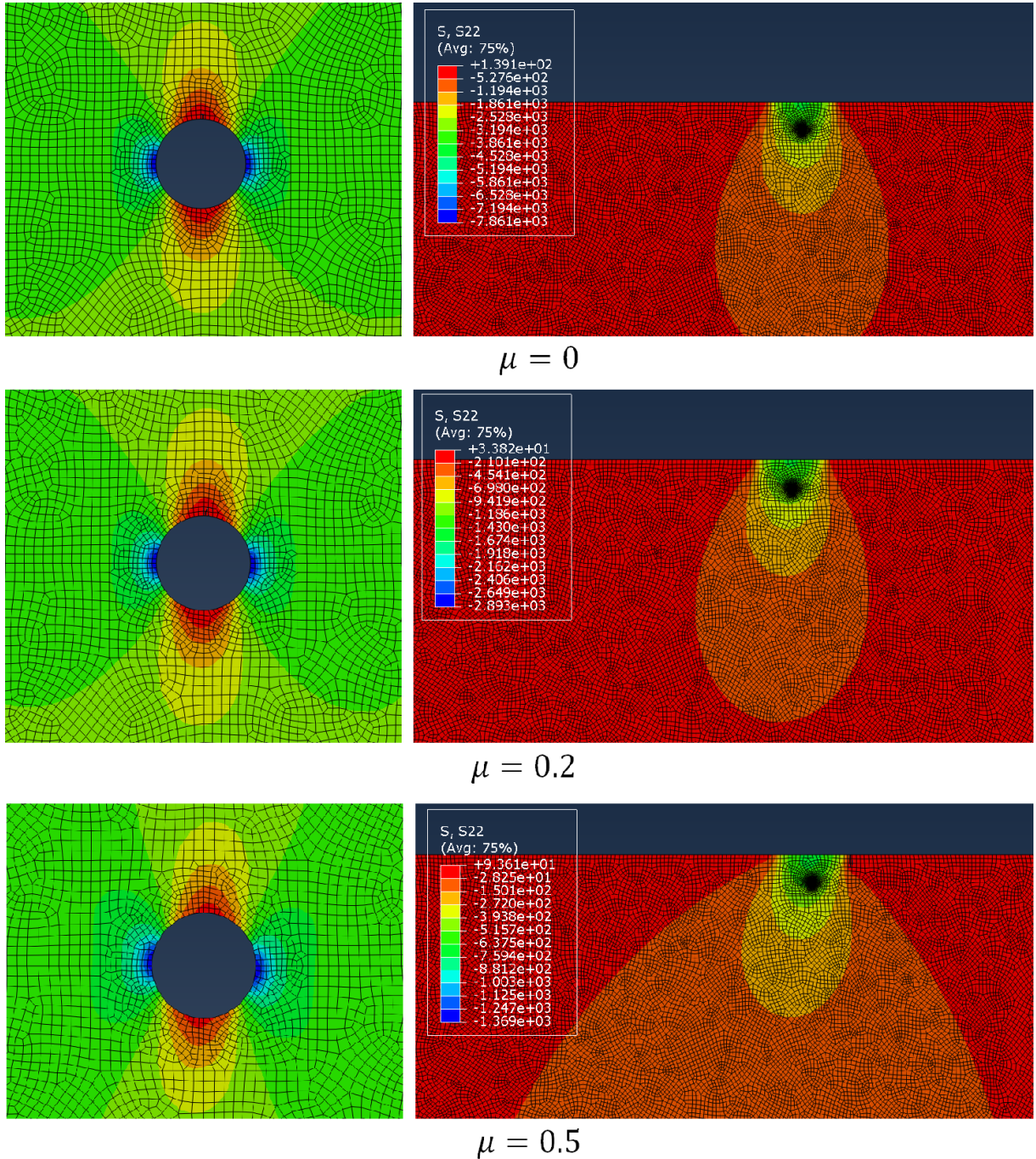


Figure 19: The σ_{yy} stress distribution for different friction values.

When crack tips were placed on the sides of the inclusion and were allocated as a crack (manual crack location) the crack did not propagate further than what was assigned. As explained earlier, this happens most likely because of compressive stresses and the crack will not further propagate.

One way to effectively visualise the patterns of the fractures is to use the field output request function *STATUSXFEM*, which is a scalar variable that shows the extent of damage inside an

element. Another function called *PHILSM* represents the *level set value* Φ that is used to define the location of cracks inside a body.

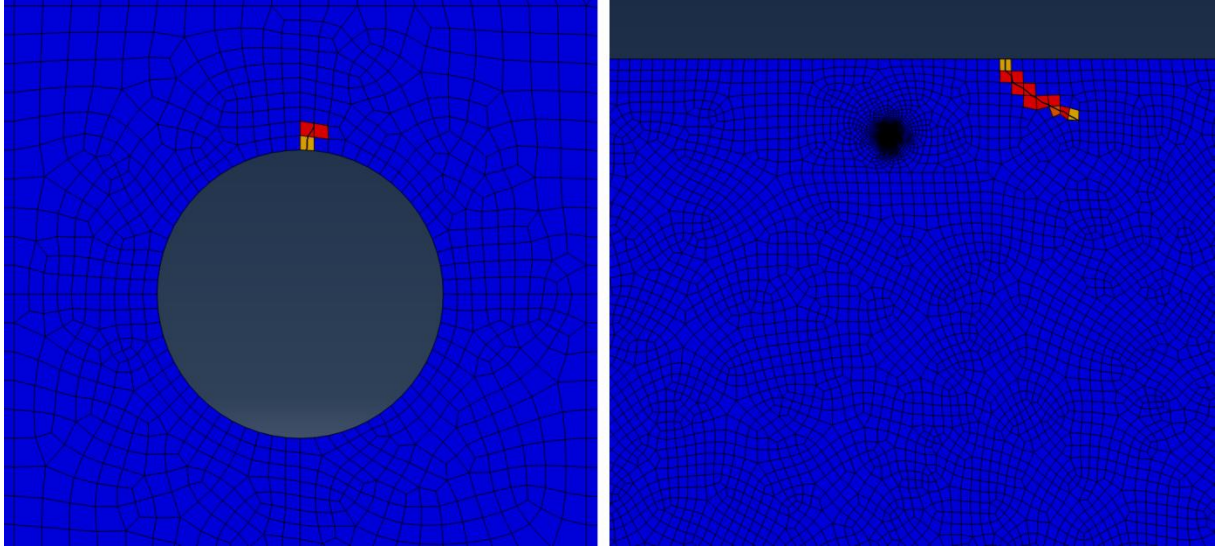


Figure 20: Crack initiations near the inclusion ($\mu = 0.2$) and at the surface ($\mu = 0.21$) with follow up propagation.

In Figure 20, crack propagation for the friction coefficient $\mu = 0.2$ and $\mu = 0.21$ respectively, is shown. A friction coefficient between these values is the critical point for when the crack starts to initiate at the surface. For all friction coefficient values $\mu \leq 0.2$, the crack initiates at the top of the inclusion. Here, it seems that the crack only propagates a few elements towards the surface for friction coefficients in the range of $\mu = 0$ to $\mu = 0.2$. There are a few reasons for why the propagation stops. It is presumably because of different options in Abaqus for instance the type of pressure distribution and magnitude selected, along with how the load is being applied, and obviously the properties of the material. Convergence difficulties of the simulations have also been a problem and one of the reasons why the propagation stops after a while.

When the friction coefficient is increased above 0.2, interesting things start to happen. Firstly, it seems that Abaqus predicts longer extensions of the crack after around $\mu = 0.5$ before sometimes stumbling upon convergence problems, which makes the simulation stop. Attempts to reduce the convergence problems have been made through implementing *automatic stabilization* as well as *discontinuous analysis* for the time increments for the static step in order to allow for additional number of attempts when a solution is converging poorly. Nonetheless, the most interesting phenomenon that follows is that the angle of which the propagation pursues increases relative to the surface as the friction coefficient is increased above 0.2, as can be seen in Figure 21. All the surface cracks seem to all initiate just outside to the right of the contact surface where the pressure distribution and traction are being applied. The reason for this initiation location can be because of a phenomenon called tearing, which occurs due to a discontinuous application of traction. Just outside to the right of the contact surface there is no pressure or traction being applied. However, just inside the contact patch on the right side there is both a pressure distribution as well as traction with direction to

the left. This coaction is a discontinuity which induces a tearing effect that appears right at the end of the contact surface to the right. What would be expected from the theory given in chapter 3.1 *Hertzian line contact in full-slip*, is that the fracture would emerge at the surface from the centre of the contact patch, at least for friction values equal to and above 0.4. The reason being, the maximum principal shear stress is located at the surface very close to the middle of the contact patch for friction values of 0.4 and above, see chapter 3.1.

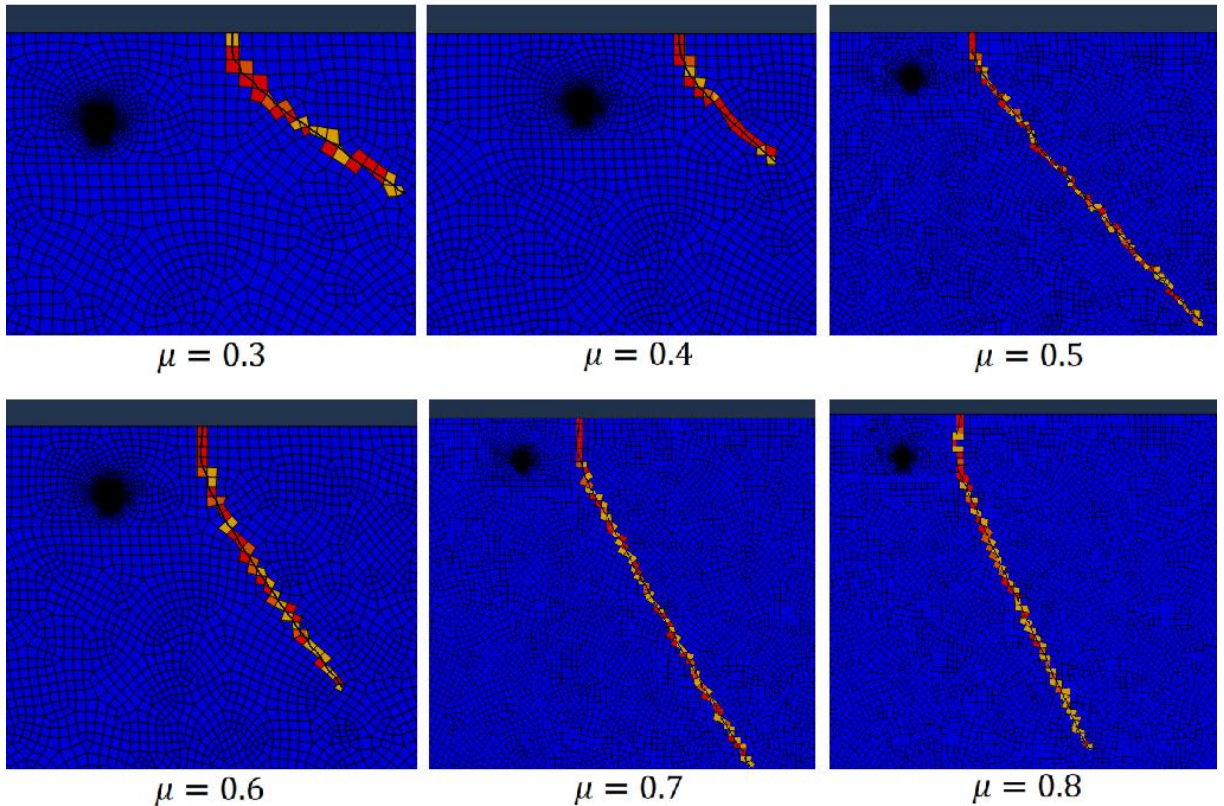


Figure 21: Cracks initiated at the surface and propagated with different friction coefficients.

When the friction coefficient reaches $\mu = 1.0$, the angle is relatively close to 90 degrees, as can be seen in Figure 22.

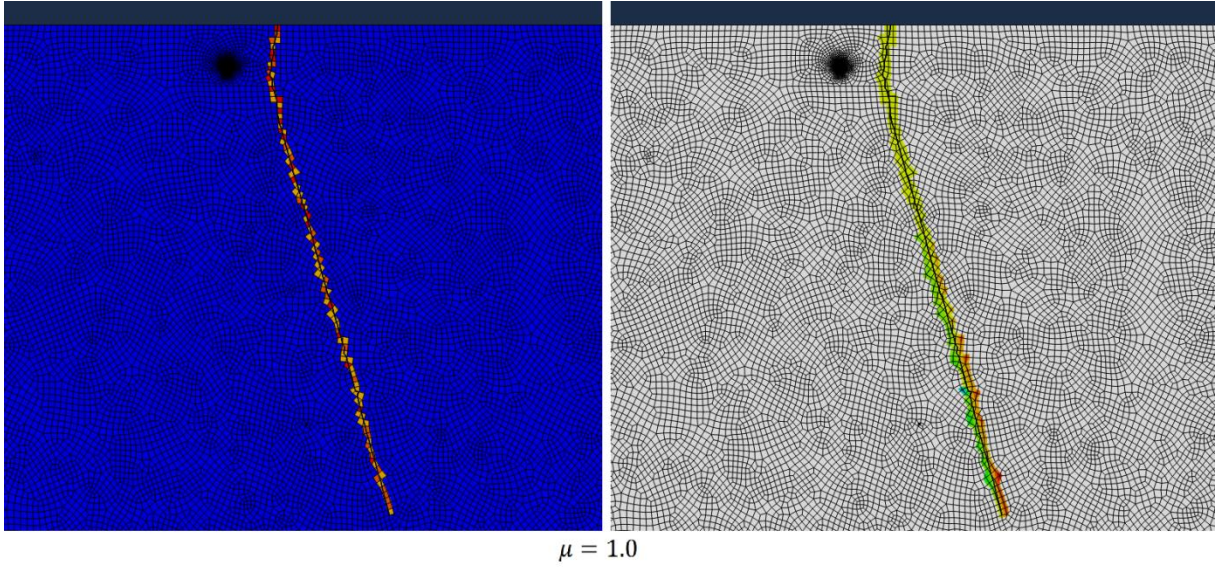


Figure 22: Crack propagation in the case of pressure distribution and traction being of equal magnitude ($\mu = \mathbf{1.0}$), which result in a fracture pattern with a very steep angle. Left: the XFEM output function. Right: the PHILSM output function.

6.2 3D Model

The situation of the crack propagation for the 3D model is quite similar to the 2D model where the crack propagates just a few elements (at the top of the inclusion) in height for friction coefficients up to 0.2. However, a broader region of several elements in x -direction is propagated here compared to the 2D model's only one element in the same direction. Figure 23 illustrates the crack propagation at the top of the inclusion for $\mu = 0.2$. The difference between the 2D and 3D model in this aspect might be due to the difference in fracture toughness (which in turn is due to higher thickness for the 3D model).

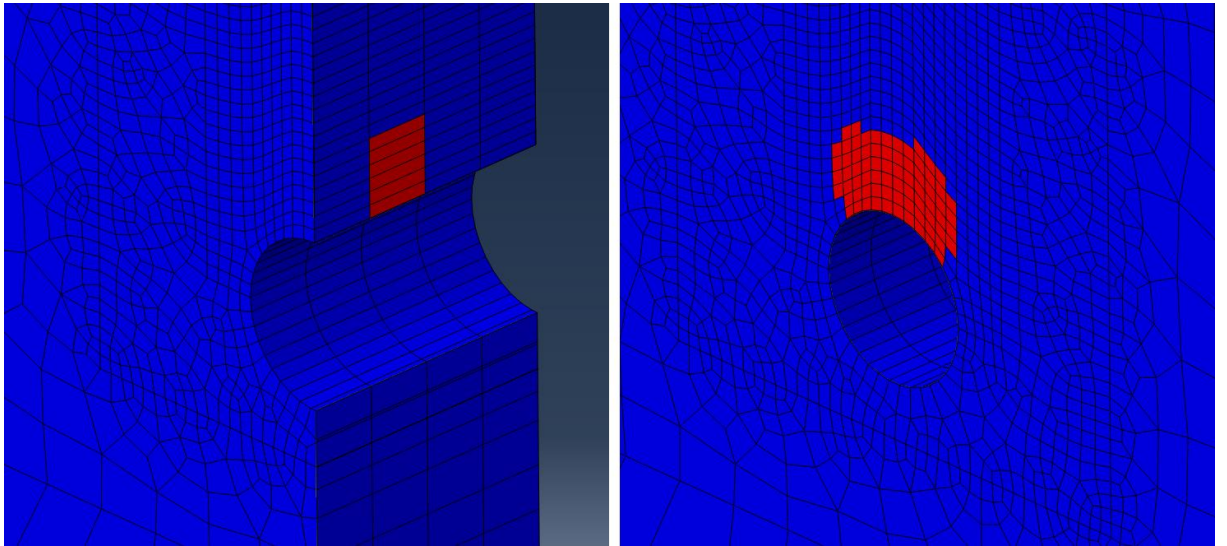


Figure 23: Crack propagation at the top of the inclusion for $\mu = \mathbf{0.2}$.

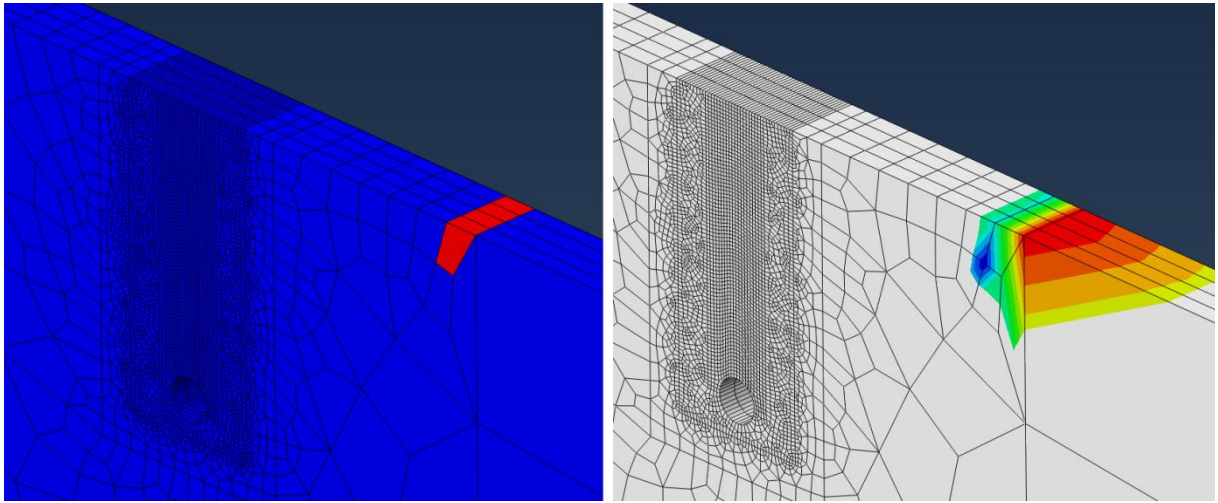


Figure 24: Crack propagation at the surface for $\mu = 0.5$ in the form of STATUSXFEM (left) and PHILSM (right).

When the friction coefficient is raised above 0.2, the crack starts to initiate at the surface, just like for the 2D model. In Figure 24, an example of a small propagation of a crack at the surface is visualised for $\mu = 0.5$. Even though the surface crack seems to initiate at the same location in general, the extension is nevertheless just one element. The main reason for this is that the simulation got into convergence problems and stopped unexpectedly.

6.3 General

The fracture mechanics method that has been used here in Abaqus is a cohesive segment approach based on XFEM. The other alternative is to use the LEFM method with VCCT for fracture analysis. This linear elastic fracture method is only valid when crack lengths are larger compared to the plastic zone size. Since no inelastic behaviours of the material has been considered, both the methods should be reasonable to use with decent accuracy. However, an elasto-plastic fracture mechanics method (EPFM) would most likely have better accuracy in the case when plastic behaviour of the material wants to be considered into the fracture analysis.

The location of the inclusion has been constant for all different friction values for both the 2D and 3D model. The location for the inclusion has been where the maximum principal shear stress is located with no applied traction ($\mu = 0$). This has been employed deliberately in order to reduce the time needed to model but also the time for the simulations. Though, this is a problem when interpreting the results of the fracture patterns etc. since the inclusions are not placed at the coordinates where the maximum principal shear stress is located for higher friction values than zero. This means that the initiation and propagation of the fracture might be altered depending on where the inclusions have been placed.

There are several more potential margins of error in the simulation process apart from the ones described above. Firstly, the mesh density has certainly an impact on the quality and accuracy of the post-processing results such as stresses and patterns of a crack. The mesh

element type also definitely has an influence on the results and the higher number of nodes that the mesh type contains; generally the higher accuracy is achieved. The mesh for the 3D model is very coarse away from the inclusion and this might be the reason why the surface cracks are not propagating longer than one element. Also, the simulation increment size has been selected to 0.01 and can also affect the results if increased or reduced. It is especially undesirable to have an increment size that is too large since the resolution of the simulation and its animation will be curtailed in the form of stutter and omitted frames.

The difference in fracture toughness for the 2D model compared to the 3D model might have an impact on the propagation patterns since the propagation extends broader for the 3D model. However, it might be other explanations for this effect to occur and the difference in fracture toughness between the models would most likely be higher in the case of plastic behaviour of the material used in the simulation.

The cohesive segment approach and the LEFM VCCT method assume different procedures in order to analyse crack growth. Thus, the different XFEM methods probably give a slight difference in the results from the post-processing since the two methods are a bit different in the fundamental basis. Furthermore, the actual premise for crack initiation and further growth is specified in the damage properties of the material in the form of maximum principal stress. This chosen maximum principal stress value needs to be experimentally retrieved for different materials in different conditions and environments in order to achieve correct crack initiation and propagation.

Both the pressure distribution and the traction have without doubt large influence on the outcome in the post-process. Especially important are the assigned magnitudes of the pressure and traction. Likewise, the material properties are of paramount significance for the fracture process.

It is of great importance to solve the problems and reduce the margins of error that are mentioned in this chapter. This is further discussed in chapter 8 *future work and research*.

7 Conclusions

There are several conclusions that can be made from the simplified FE-models that have been constructed in this thesis and they are furthermore presented in this chapter.

For the 2D model, compressive stresses at the sides of the inclusion inhibit initiation of fractures, and tensile stresses at the top and bottom of the inclusion facilitates the opening of the fracture at the top. The fracture initiates at the inclusion, specifically at the top, when friction coefficients are equal to or below the value 0.2. The fracture propagates a few elements upwards in the first static cycle. For friction coefficients above the value 0.2, the fracture initiates at the surface. This occurs specifically at the boundary where the pressure distribution and traction is applied at the right side, when the traction direction is to the left. The likely cause of this fracture initiation at this surface location is tearing. The fracture propagates downwards with an angle and along a certain well-defined line. The pattern of the fracture propagation for a surface crack depends on the friction coefficient value. Specifically, the angle of a surface crack increases relative to the surface as the friction coefficient value is increased.

Compared to the 2D model, the fracture for the 3D model extends broader at the top of the inclusion in the case of friction coefficient values equal to or below 0.2. At friction coefficient values above 0.2, the fracture initiates at the same location as for the 2D model. However, the propagation is non-existent due to convergence problems.

The FE-models constructed are initial steps towards analysing the fracture propagation and closely related phenomena for a railway freight wheel in detail. This thesis can therefore be seen as a contribution to the research in the area and to reduce the accidents as well as the maintenance for railway wheels. These motives have direct positive association to the society and its economy as a whole. The potential reduction of the rate of wear of railway wheel steel is additionally less harmful for the environment. At the current stage, the simplified models give mainly information about the fracture initiation, propagation and its patterns. From this first phase, further adjustments and improvements can take place in order to eliminate the margins of error. In the long run, fully integrated models with further implementations such as detailed microstructure for the contact conditions, plastic behaviour for the material, and complete three-dimensional models can finally be employed.

8 Future Work and Research

The FE-models that have been designed in this thesis are initial work before they can be fully utilized with relation to the wear rate with contact conditions and material properties etc. Many simplifications have been made in order to achieve certain results and make progress in the given tight time frame. Most of the options that have been neglected for the time being are in Abaqus thus reasonably straightforward to implement in the case of further work and research being put into this area. From this background, it has been important to keep a balance for what is presented in this work which has inevitably lead to plenty of future potential improvements in several areas.

Firstly, by studying many sources of fracture mechanics, some state that cyclic loading can in some cases be necessary in order for the fracture to further propagate. Also, the number of load cycles has definitely an impact on the extension of a crack. The main limitation of implementing these measures are that it is time consuming but can also create problems where the errors can be more difficult to solve.

Simplifications has been made for the wheel contact in form of the Hertzian theory as well as full-slip condition. This has made the implementation of the loads in Abaqus substantially more straightforward. However, stresses, wear and fractures depends greatly on the methodologies and assumptions used, since their accuracies vary. In this case, the Hertzian theory for the normal contact problem has been shown to be not very accurate in the estimation of the shear stresses. Moreover, the full-slip condition used in this work is not realistic in all situations and therefore partial slip could be implemented and further researched in the context of creating a fracture propagation model. When speaking of reality, instead of applying a static load (or continuous cyclic loads) at the same location over and over, a moving contact pressure distribution could be applied instead, in order to simulate the wheel rolling over its inclusion or crack. This could give more detailed and accurate results in regards to for instance nucleation locations and fracture patterns. What could also change the patterns of the crack and the premises of which the cracks initiate is the depth of the inclusions or voids. Therefore, for future analyses, the determined depth of an inclusion could be varied as well as shifted in longitudinal direction in order to place the inclusions over the areas of where the principal shear stress is maximum for when the friction coefficient $\mu > 0$. It can be difficult to generate a failure of the material in form of a delamination process if only one crack initiates at the top of the inclusion and then propagates to the surface. Therefore, for the sake of trying to simulate a removal of a particle from the surface, deliberate and manual placements of cracks can be done, for instance two above of the inclusion with a certain angle that separate them.

Again, because of streamlining the work in order to be able to get some initial results in time, only elastic material properties has been used. This has been especially effective due to the adoption of XFEM in Abaqus for the crack propagation approach since it uses linear elastic fracture mechanics methods. However, to be able to account for the plasticity of a material,

especially around the crack tips, an elasto-plastic fracture mechanics method is needed. Though, this method is not as well implemented into FE-software as the LEFM is.

There are improvements that can be made for the boundary conditions applied in the models. More accurate solutions are most likely for instance absorbing boundary conditions or infinite boundaries that will absorb the energy at the boundaries which the pressure applied at the contact patch releases.

For all the different models constructed in this work, from two dimensions to three, finer mesh is needed in order to increase the accuracy of the stresses calculated in the bulk of the material, especially near the inclusions or the crack tips. Yet, for three dimension models, this is notably more computationally expensive compared to two dimension models. This creates the demand of powerful computers in order to reduce the simulation time. Aside from increasing the resolution of the mesh, a mesh element type with many nodes is also very important to select in order to achieve a higher precision in the stresses.

In order to for instance change direction of traction and propagate cracks in a 3D domain, a full 3D model can be constructed. This would open up to more complex results as well as more possibilities for alterations of different settings in Abaqus.

A large step towards developing the models is to take the asperities and the surface roughness into account in the contact of the wheel and rail. This can be done through the microstructural analysis of different wear mechanisms done by CAF MiiRA. The fracture propagation models should be able to be utilized in companies and for future research if further development is ensued adhering to the above.

References

- [1] <https://shift2rail.org/about-shift2rail/>, last visited 2018-08-03.
- [2] http://projects.shift2rail.org/s2r_ip5_n.aspx?p=FR8RAIL, last visited 2018-08-03.
- [3] B. Dirks, Vehicle dynamics simulation of wheel wear for Swedish high-speed train X2000, 2003.
- [4] S. Hossein-Nia, On Heavy-Haul Wheel Damages using Vehicle Dynamics Simulation, 2018.
- [5] R. G. Bayer, Wear Analysis for Engineers, 2002.
- [6] I. M. Hutchings, Tribology – Friction and Wear of Engineering Materials, 1992.
- [7] N. P. Suh, An overview of the delamination theory of wear, *Wear*, Volume 44, Issue 1, 1977, Pages 1-16.
- [8] D. Roylance, Introduction to Fracture Mechanics, 2001.
- [9] P. Davy, R. L. Goc and C. Darcel, A model of fracture nucleation growth and arrest and consequences for fracture density and scaling, *Journal of Geophysical Research: Solid Earth*, Volume 118, Issue 4, 2013.
- [10] S. A. G. Oliveira and A. F. Bower, An analysis of fracture and delamination in thin coatings subjected to contact loading, *Wear*, Volume 198, Issues 1-2, 1996, Pages 15-32.
- [11] Spiestersbach et al, Crack initiation mechanisms and threshold values of very high cycle fatigue failure of high strength steels, *Procedia Engineering*, Volume 74, 2014, Pages 84-91.
- [12] M. Zhu and F. Xuan, Fatigue Crack Initiation Potential from Defects in terms of Local Stress Analysis, *Chinese Journal of Mechanical Engineering*, Volume 27, Issue 3, 2014, Pages 496-503.
- [13] A. Ekberg, Rolling contact fatigue on railway wheels, 2000.
- [14] Y. Murakami and M. Endo, Effects of defects, inclusions and inhomogeneities on fatigue strength, *International Journal of Fatigue*, Volume 16, Pages 163-182, 1994.
- [15] Y. Murakami, S. Kodama and S Konuma, Quantitative evaluation of effects of non-metallic inclusions on fatigue strength of high strength steels. I: basic fatigue mechanism and evaluation of correlation between the fatigue fracture stress and the size and location of non-metallic inclusions, *International Journal of Fatigue*, Volume 11, Pages 291-298, 1989.
- [16] https://en.wikipedia.org/wiki/Fracture_mechanics, last visited 2018-08-03.
- [17] E 399-83, Standard Test Method for Plane-Strain Fracture Toughness of Metallic Materials, ASTM, 1983.
- [18] T. Belytschko and T. Black, Elastic Crack Growth in Finite Elements with Minimal Remeshing, *International Journal for Numerical Methods in Engineering*, 45, 1999, Pages 601-620.
- [19] S. Jiang, Z. Ying and C. Du, The optimal XFEM approximation for fracture analysis, *IOP Conference Series: Materials Science and Engineering*, Volume 10, Number 1, 2010.
- [20] E. Giner, N. Sukumar, J. E. Tarancón and F. J. Fuenmayor, An Abaqus implementation of the extended finite element method, *Engineering Fracture Mechanics*, 76, 2009, Pages 347-368.
- [21] K. L. Singh, K. Keswani and M. Vaggar, Crack growth simulation of stiffened fuselage panels using XFEM techniques, *Indian Journal of Engineering & Materials Sciences*, Volume 21, 2014, Pages 418-428.
- [22] <https://www.3ds.com/products-services/simulia/products/>, last visited 2018-08-03.

TRITA-SCI-GRU 2018:321
ISBN 978-91-7729-905-9